AD-A197 639

MODE COUPLING IN VLF/LF ATMOSPHERIC NOISE MODELS

C. R. Warber
E. C. Field, Jr.
Pacific-Sierra Research Corporation
12340 Santa Monica Boulevard
Los Angeles, CA 90025-2587

31 August 1987

Technical Report

Prepared for
    Director
    DEFENSE NUCLEAR AGENCY
    Washington, DC 20305-1000

88 7 26 048

AD-A197 639

REPORT DOCUMENTATION PAGE

1a. REPORT SECURITY CLASSIFICATION	1b. RESTRICTIVE MARKINGS
UNCLASSIFIED	

2a. SECURITY CLASSIFICATION AUTHORITY	3. DISTRIBUTION/AVAILABILITY OF REPORT
N/A since Unclassified	Approved for public release; distribution is unlimited.
2b. DECLASSIFICATION/DOWNGRADING SCHEDULE	
N/A since Unclassified	

4. PERFORMING ORGANIZATION REPORT NUMBER(S)	5. MONITORING ORGANIZATION REPORT NUMBER(S)
PSR Report 1725	DNA-TR-87-169

6a. NAME OF PERFORMING ORGANIZATION	6b. OFFICE SYMBOL (If applicable)	7a. NAME OF MONITORING ORGANIZATION
Pacific-Sierra Research Corporation		Director Defense Nuclear Agency

6c. ADDRESS (City, State, and ZIP Code)	7b. ADDRESS (City, State, and ZIP Code)
12340 Santa Monica Boulevard Los Angeles, CA 90025-2587	Washington, DC 20305-1000

8a. NAME OF FUNDING/SPONSORING ORGANIZATION	8b. OFFICE SYMBOL (If applicable)	9. PROCUREMENT INSTRUMENT IDENTIFICATION NUMBER
	RAAE/Emmes	DNA 001-85-C-0105

8c. ADDRESS (City, State, and ZIP Code)	10. SOURCE OF FUNDING NUMBERS			
	PROGRAM ELEMENT NO	PROJECT NO	TASK NO	WORK UNIT ACCESSION NO
	62715H	RB	RB	DH008655

11. TITLE (Include Security Classification)

MODE COUPLING IN VLF/LF ATMOSPHERIC NOISE MODELS

12. PERSONAL AUTHOR(S)
Warber, C. R.; Field, E. C. Jr.

13a. TYPE OF REPORT	13b. TIME COVERED	14. DATE OF REPORT (Year, Month, Day)	15. PAGE COUNT
Technical	FROM 850123 TO 870626	870831	78

16. SUPPLEMENTARY NOTATION
This work was sponsored by the Defense Nuclear Agency under RDT&E RMC Code
B3220854662 RB RB 00047 25904D. *from 15*

17.	COSATI CODES		18. SUBJECT TERMS (Continue on reverse if necessary and identify by block number)
FIELD	GROUP	SUB-GROUP	VLF/LF Propagation ; Strategic Communication ;
25	2		Ground Conductivity ; Waveguide (φ/rh)
20	1		Long-Wave Communication

19. ABSTRACT (Continue on reverse if necessary and identify by block number) *are derived and tested*

- PSR derives and tests tractable formulas for coupling among VLF/LF waveguide modes that occurs at boundaries separating regions of different ground conductivity. Although algebraically complicated, the formulas are easily programmed and require less computer running time than numerical mode-coupling algorithms used in "exact" computer codes.
The formulas have two desirable features; (1) computational simplicity and (2) dependence on ground conductivity on either side of a transition (while depending only slightly on the conductivity variation within the transition itself).

The formulas are subjected to three approximations, valid under most circumstances: (1) substitution of an equivalent parallel-plate waveguide for the actual waveguide in the short spatial interval that contains the conductivity boundary, (2) application of the WKB approximation, requiring that all conductivity changes in the transition zone be gradual (occurring over at least 1/6 wavelength), and (3) neglection of phase (only the magnitudes of the modes are used when performing certain numerical operations).

20. DISTRIBUTION/AVAILABILITY OF ABSTRACT	21. ABSTRACT SECURITY CLASSIFICATION
☐ UNCLASSIFIED/UNLIMITED ☒ SAME AS RPT. ☐ DTIC USERS	UNCLASSIFIED

22a. NAME OF RESPONSIBLE INDIVIDUAL	22b. TELEPHONE (Include Area Code)	22c. OFFICE SYMBOL
Sandra E. Young	(202) 325-7042	DNA/CSTI

DD FORM 1473, 84 MAR

83 APR edition may be used until exhausted.
All other editions are obsolete.

SECURITY CLASSIFICATION OF THIS PAGE
UNCLASSIFIED

19. ABSTRACT (Continued)

Although derived for inclusion in future computer models of VLF/LF worldwide atmospheric noise, the mode-coupling formulas can be used in any application involving such a large number of propagation paths that the length of computer running time becomes a problem. *Keywords:* → *fields?*

SUMMARY

This report derives and tests tractable approximate formulas for coupling among very low frequency/low frequency (VLF/LF) waveguide modes that occurs at boundaries that separate regions having different ground conductivity. Although algebraically complicated, these formulas are easily programmed and require far less computer running time than the numerical mode-coupling algorithms used in full wave computer codes.

To derive and implement the formulas, we substitute an equivalent parallel-plate waveguide for the actual waveguide in the short spatial interval that contains the conductivity boundary. This approximation is most easily applied to daytime ionospheric conditions. We derive a set of coupled differential equations which have as their first-order solution the well-known Wentzel-Kramers-Brillouin (WKB) approximation. However, in contrast to the WKB solution, the method of the present report gives results beyond the first-order and obtains solutions to any order necessary to achieve specified accuracy. Although derived for inclusion in future computer models of VLF/LF worldwide atmospheric noise, the mode-coupling formulas could be used in applications where a large number of propagation paths cause computer running time to become a problem.

PREFACE

To assess the performance of long-wave communication links in nuclear environments, it is necessary to calculate the effect of the environment on atmospheric noise as well as on the signal. Because no data for atmospheric noise exist under nuclear-disturbed conditions, the Defense Nuclear Agency is considering developing a computer model that will predict the noise. A major difficulty in implementing such a model is developing an accurate, yet tractable, means of calculating coupling between waveguide modes over geologically complex regions like Canada and Greenland. Accordingly, the present report develops and tests mode-coupling formulas suitable for inclusion in future noise models.

CONVERSION TABLE

Conversion factors for U.S. Customary to metric (SI) units of measurement

MULTIPLY ——————→ BY ——————→ TO GET
TO GET ←—————— BY ←—————— DIVIDE

angstrom	1.000 000 X E -10	meters (m)
atmosphere (normal)	1.013 25 X E +2	kilo pascal (kPa)
bar	1.000 000 X E +2	kilo pascal (kPa)
barn	1.000 000 X E -28	$meter^2$ (m^2)
British thermal unit (thermochemical)	1.054 350 X E +3	joule (J)
calorie (thermochemical)	4.184 000	joule (J)
cal (thermochemical)/cm^2	4.184 000 X E -2	mega joule/m^2 (MJ/m^2)
curie	3.700 000 X E +1	*giga becquerel (GBq)
degree (angle)	1.745 329 X E -2	radian (rad)
degree Fahrenheit	$t_K = (t°f + 459.67)/1.8$	degree kelvin (K)
electron volt	1.602 19 X E -19	joule (J)
erg	1.000 000 X E -7	joule (J)
erg/second	1.000 000 X E -7	watt (W)
foot	3.048 000 X E -1	meter (m)
foot-pound-force	1.355 818	joule (J)
gallon (U.S. liquid)	3.785 412 X E -3	$meter^3$ (m^3)
inch	2.540 000 X E -2	meter (m)
jerk	1.000 000 X E +9	joule (J)
joule/kilogram (J/kg) (radiation dose absorbed)	1.000 000	Gray (Gy)
kilotons	4.183	terajoules
kip (1000 lbf)	4.448 222 X E +3	newton (N)
kip/$inch^2$ (ksi)	6.894 757 X E +3	kilo pascal (kPa)
ktap	1.000 000 X E +2	newton-second/m^2 $(N-s/m^2)$
micron	1 000 000 X E -6	meter (m)
mil	2.540 000 X E -5	meter (m)
mile (international)	1.609 344 X E +3	meter (m)
ounce	2.834 952 X E -2	kilogram (kg)
pound-force (lbs avoirdupois)	4.448 222	newton (N)
pound-force inch	1.129 848 X E -1	newton-meter (N·m)
pound-force/inch	1.751 268 X E +2	newton/meter (N/m)
pound-force/$foot^2$	4.788 026 X E -2	kilo pascal (kPa)
pound-force/$inch^2$ (psi)	6.894 757	kilo pascal (kPa)
pound-mass (lbm avoirdupois)	4.535 924 X E -1	kilogram (kg)
pound-mass-$foot^2$ (moment of inertia)	4.214 011 X E -2	kilogram-$meter^2$ $(kg·m^2)$
pound-mass/$foot^3$	1.601 846 X E +1	kilogram/$meter^3$ (kg/m^3)
rad (radiation dose absorbed)	1.000 000 X E -2	**Gray (Gy)
roentgen	2.579 760 X E -4	coulomb/kilogram (C/kg)
shake	1.000 000 X E -8	second (s)
slug	1.459 390 X E +1	kilogram (kg)
torr (mm Hg, 0°C)	1.333 22 X E -1	kilo pascal (kPa)

*The becquerel (Bq) is the SI unit of radioactivity; 1 Bq = 1 event/s.
**The Gray (Gy) is the SI unit of absorbed radiation.

TABLE OF CONTENTS

SECTION 1

INTRODUCTION

Electromagnetic signals or noise at frequencies below 60 kHz consist of a number of waveguide modes that propagate in a cavity bounded sharply on the bottom by the earth and diffusely on the top by the ionosphere. The excitation and propagation of those modes depend on the electrical properties of the earth and ionosphere. For uniform paths, such as a midday path over seawater, the modes propagate more or less independently of one another. However, on so-called mixed paths, along which the properties of either the earth or the ionosphere change, the modes become interdependent. That process is called mode coupling and is strongest near transition zones, where geophysical changes are most pronounced.

The most common and severe transition zones in the earth-ionosphere waveguide are at the boundaries that separate large regions of dissimilar ground conductivity. Other transitions are at the terminator and at the edges of ionospheric regions subjected to solar-induced or nuclear disturbances. This report mainly addresses ground conductivity transitions, although the methods developed here are also applicable to other types.

Waveguide transitions can be modeled as being either gentle or abrupt, depending on whether they occur over distances that are longer or shorter, respectively, than about one-sixth of the signal wavelength. Gentle transitions cause only slight mode coupling, whereas abrupt ones cause strong coupling. In the 15 to 60 kHz band considered here, one-sixth of a wavelength never exceeds 3 km.

Both the WAVEGUID code (developed by the Naval Ocean Systems Center, San Diego, California) and the WAVEPROP code (developed by Pacific-Sierra Research Corporation) can handle mode coupling on mixed paths having either gentle or abrupt transitions. Data are sparse, however; and, for lack of better information, geological maps ˙sed for this purpose show discontinuous ground-conductivity transitio s [Westinghouse, 1968]. The codes, therefore, treat conductivity

transitions as abrupt. In fact, conductivity transitions probably occur over distances of several kilometers or more and should, therefore, be treated as gentle.

Propagation codes, which are always expensive to run, are especially costly for paths that traverse geophysically complex regions, such as Canada. Although that expense is often manageable, it can become overwhelming if the number of paths is large. A case in point is prediction of low-frequency atmospheric noise, which is modeled by calculating the energy that propagates from several hundred worldwide noise sources. The number of propagation paths in that case is enormous, and inclusion of a full-fledged, mode-coupling matrix at each conductivity boundary is out of the question. Simplified equations are needed to make such calculations tractable.

The present report addresses the problem of atmospheric noise modeling. In order to derive mode-coupling formulas that are inexpensive to compute, we make three main assumptions. First, because the conductivity transitions occur over distances much shorter than the earth's radius, we use a parallel-plate waveguide to model the earth and ionosphere. That assumption allows calculation of mode parameters from transcendental, rather than differential equations. It is more easily applied to daytime or disturbed conditions, where propagation is nearly isotropic, than to nighttime conditions, where the ionosphere is diffuse and isotropic and therefore more difficult to model as a conductivity half-space. This report does not address nighttime propagation. Second, we use a generalized Wentzel-Kramers-Brillouin (WKB) method to determine the fields. That method is more accurate than the usual WKB solutions (see for example Budden, 1985). The main validity criterion is that the change in conductivity is gentle enough that reflections of the modes can be neglected. The appendix shows that criterion to be well satisfied. The third and final assumption is that relatively few modes need be retained. That assumption is valid because noise bursts are incoherent, and phase need not be kept in mode summation (but is kept elsewhere). There is thus no need to keep many high-order modes, which are usually included in computing coherent signals to ensure that "nulls" are calculated correctly.

2

The new formulas connect long-wave fields on opposite sides of waveguide transitions and are in a form that can be used in future noise models. They require much less computer time than equations now used in sophisticated propagation codes; and they provide accuracy at least commensurate with--and probably better than--the accuracy of the input data.

SECTION 2
TRANSITIONS IN GROUND CONDUCTIVITY

In this section, we discuss ground conductivity maps used for long-wave propagation calculations. We also present sample data showing that substantial approximations can be made in computing mode coupling at conductivity boundaries.

CONDUCTIVITY MAPS.

Long-wave propagation does not depend strongly on conductivity over regions where the conductivity exceeds approximately 3×10^{-3} S/m, because ground having such high conductivity reflects very low frequency/low frequency (VLF/LF) waves almost perfectly. For that reason, only slight mode coupling occurs at a boundary separating two regions of high conductivity. However, ground conductivities below about 10^{-3} S/m strongly affect the excitation and propagation of transverse magnetic (TM) signals in the VLF and LF bands, and can affect excitation of transverse electric (TE) signals. Such low conductivities occur in Greenland and Northeastern Canada, as well as certain other regions, including parts of the Soviet Union.

Figure 1 is an example of the conductivity maps used in long-wave propagation calculations [Westinghouse, 1968]. It shows VLF conductivity values throughout most of North America. Analogous maps exist for virtually all regions of the earth. The map divides Canada into a number of large regions, with uniform conductivity assigned to each. The regions are separated by abrupt boundaries.

Maps such as that in Fig. 1 are based on sparse data. There is particularly little information about remote areas like Northern Canada; for those regions, confidence in the conductivity values is low [Westinghouse, 1968]. Although such maps are useful for inferring average ground conductivity over long propagation path segments, their resolution is not good enough to define the structure within boundaries that separate adjacent regions. The boundaries shown on the maps are, therefore, not based on data, and are portrayed as abrupt

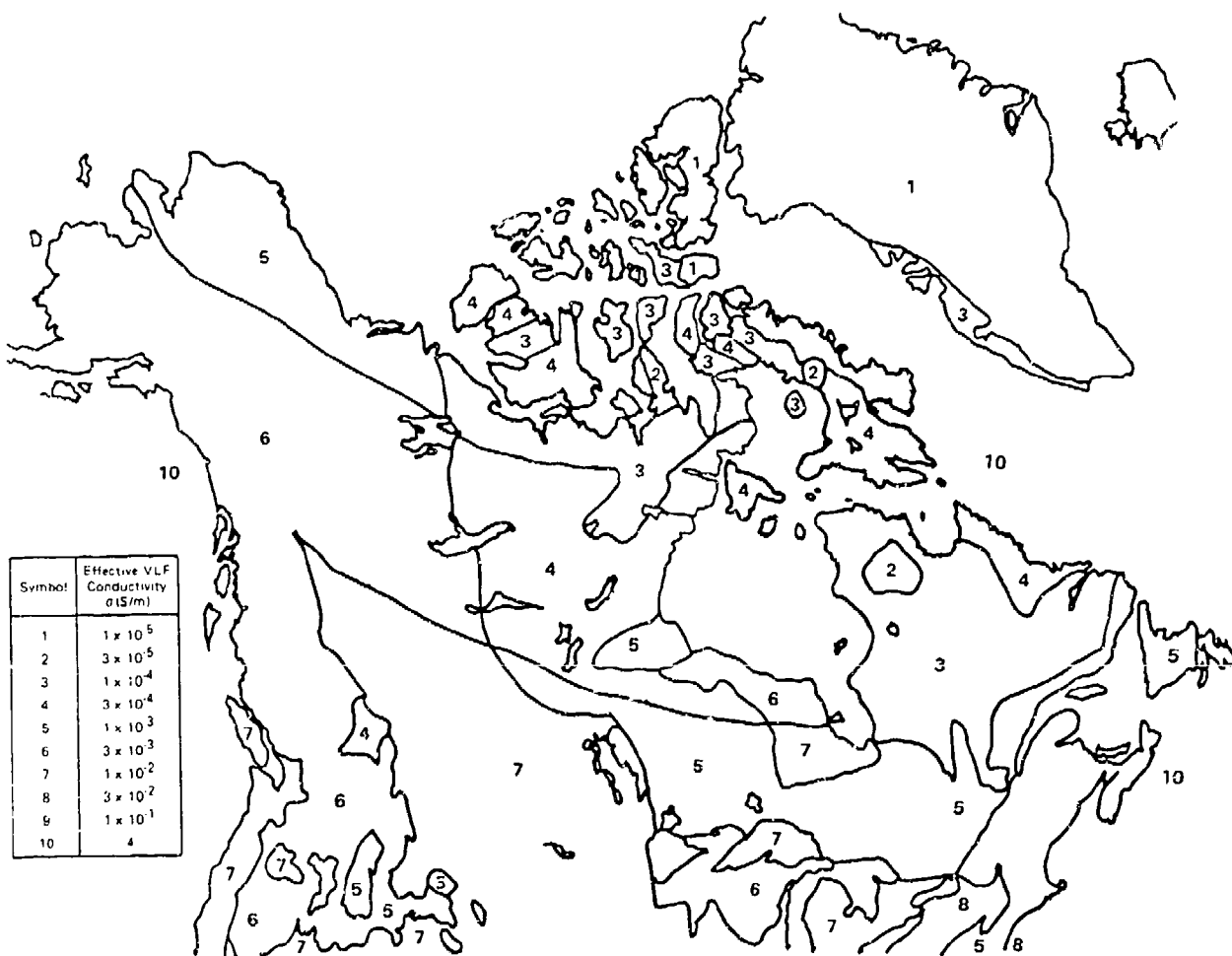| Symbol	Effective VLF Conductivity σ (S/m)
1	1×10^{-5}
2	3×10^{-5}
3	1×10^{-4}
4	3×10^{-4}
5	1×10^{-3}
6	3×10^{-3}
7	1×10^{-2}
8	3×10^{-2}
9	1×10^{-1}
10	4

Figure 1. Effective ground-conductivity regions in Northern U.S. and Canada.

5

simply for ease of presentation. Since other models are unavailable, conductivity maps like that shown are used as inputs to long-wave propagation codes.

We assert that conductivity transitions--although abrupt on the scale of a continent--are probably rather gentle on the scale of a wavelength. Transition zones between conductivity regions should, therefore, be modeled as gradual rather than as sharp boundaries.

EFFECTIVE AND BULK GROUND CONDUCTIVITIES.

The electrical conductivity of the earth varies with depth, so the effective ground conductivity "seen" by a wave in the earth-ionosphere waveguide is an average over about a skin-depth δ from the surface. Because the skin depth depends on wave frequency, the effective ground conductivity exhibits a weak frequency dependence. The map shown in Fig. 1, for example, applies to frequencies from 10 to 30 kHz.

Figure 2 shows skin depth versus frequency for several values of ground conductivity σ [Kraichman, 1970]. The VLF/LF communication bands are indicated by the shaded regions on the right side of the figure. For normal ground, where σ lies between 10^{-2} and 10^{-3} S/m, the VLF/LF skin depths lie between about 30 to 100 m; for poorly conducting ground, where σ lies between about 10^{-4} and 10^{-5} S/m, the skin depths lie between about 300 to 1000 m.

Of all the conductivity boundaries shown in Fig. 1, those at shorelines are expected to be the most abrupt. To examine that behavior, we use the data given in Fig. 3, which shows measured bulk conductivity versus distance inland on the Olympic Peninsula in Northwest Washington State [Bostick, Smith, and Boehl, 1977]. Although not measured at a low-conductivity site, the data are among the few available that illustrate the spatial dependence of conductivity near a boundary.

Figure 1 shows that the effective conductivity of the Olympic Peninsula is 10^{-2} S/m, which implies that depths within several tens of meters from the surface contribute to the conductivity. Figure 3 shows in detail, on the other hand, that at such depths the
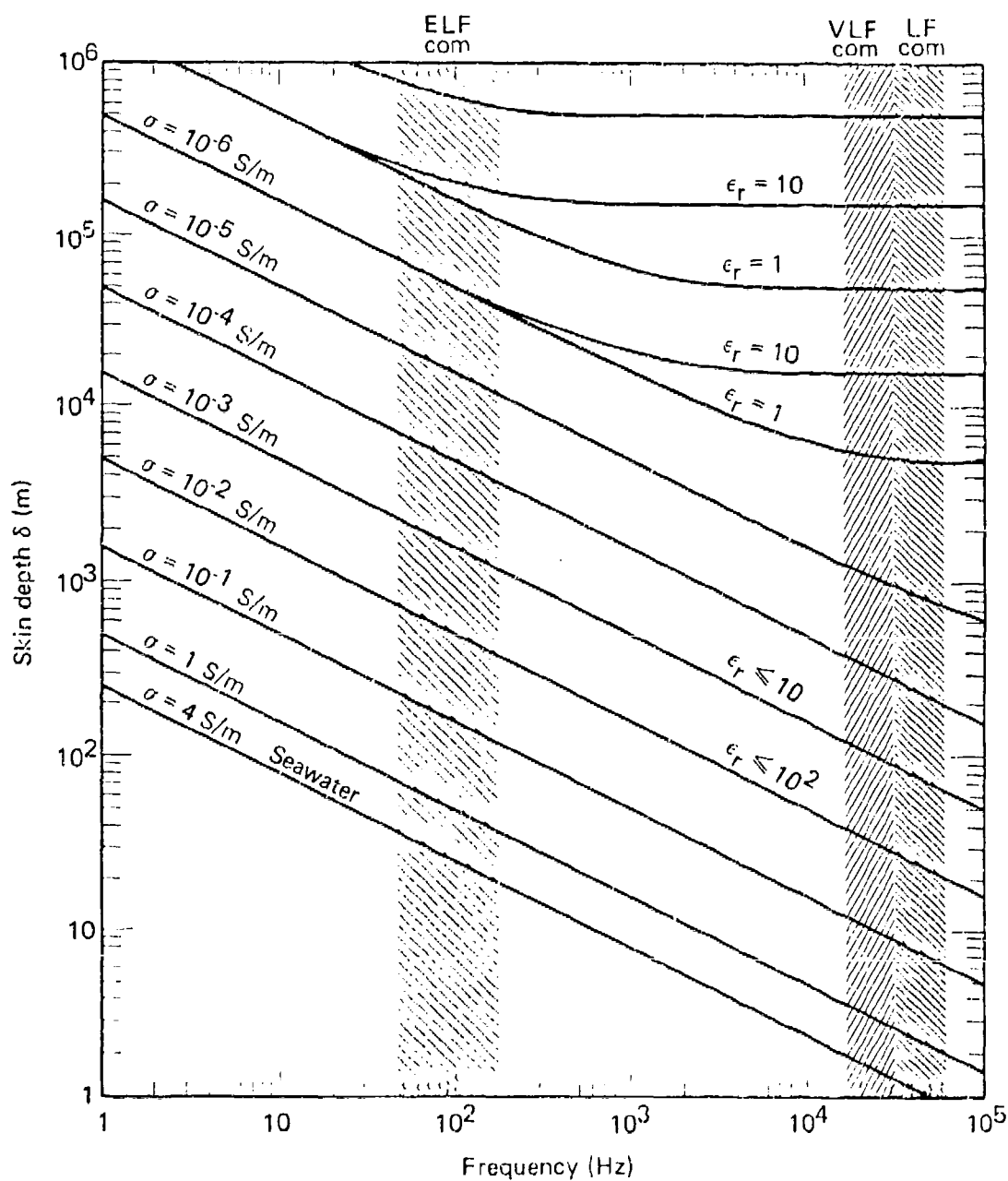
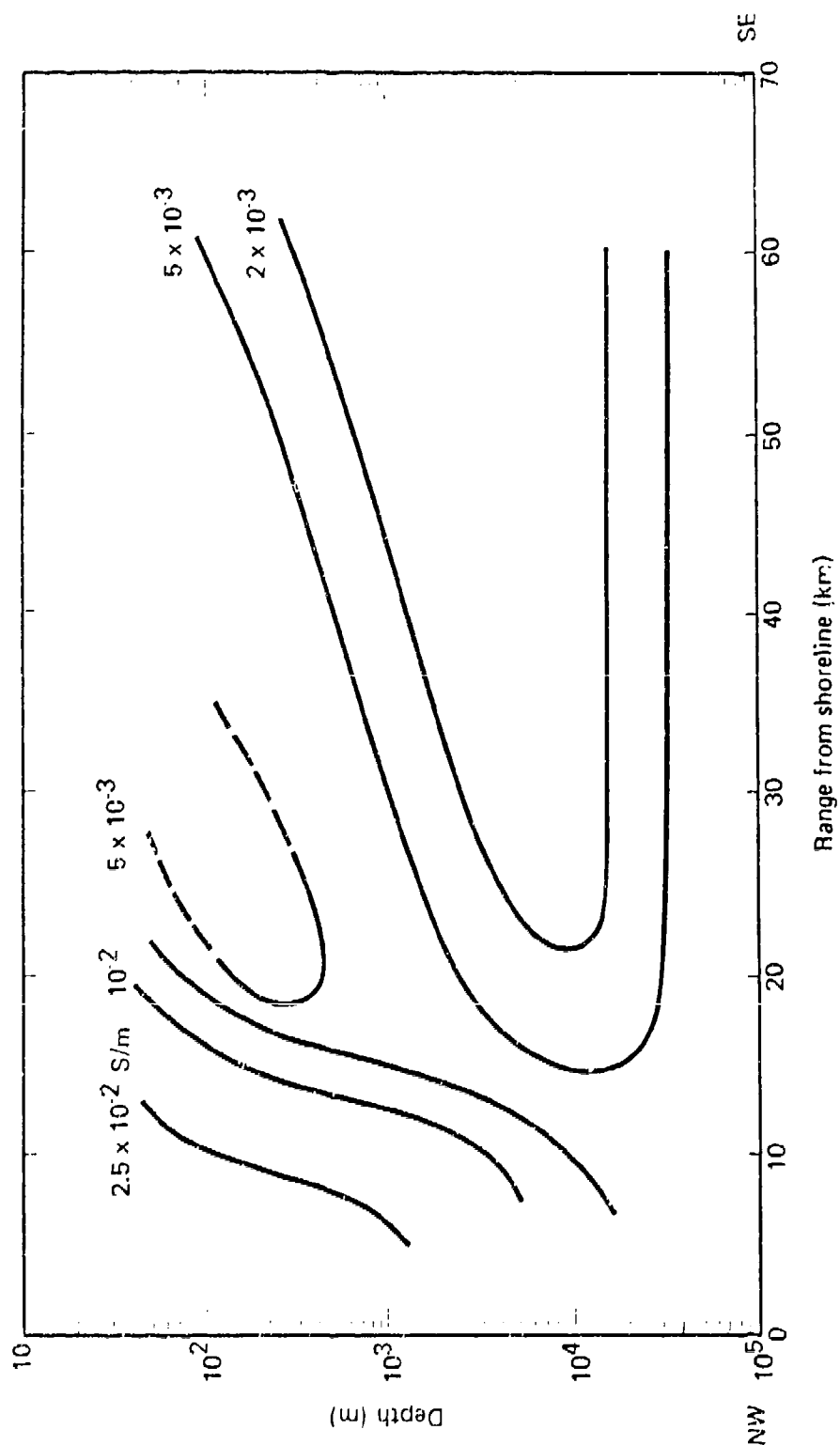Figure 2. Skin depth versus frequency for various conductivities σ and relative permittivities ϵ_r.

Figure 3. Transverse section of estimated true conductivity on Olympic Peninsula.

8

conductivity is about 5×10^{-3} S/m at distances more than 20 km from the shoreline, and increases as the shoreline is approached. The conductivity is presumably 4 S/m on the sea side of the shoreline, but no data were measured there.

We draw two conclusions from Fig. 3. First, the inland effective conductivity on the Olympic Peninsula ($\sigma \approx 5 \times 10^{-3}$ S/m) is within a factor of 2 of the nominal value ($\sigma \approx 10^{-2}$ S/m) given on the large-scale conductivity map. Considering the sparse data on which the maps are based, such accuracy is as good as can be expected. Second, at least on the Olympic Peninsula, the effective ground conductivity requires more than 10 km to transition from its shoreline value to its inland value. Although those data are site-specific, we assert that qualitatively similar behavior occurs at other sites (where data are not available), and that even more gradual transitions probably occur between the inland regions depicted in Fig. 1.

FULL-WAVE CALCULATION OF FIELDS AT TRANSITIONS.

The WAVEGUID [Pappert and Shockey, 1972; Pappert, Moler, and Shockey, 1970] and WAVEPROP [Field et al., 1976] codes calculate waveguide mode parameters numerically, accounting for (1) the vertical inhomogeneity of the ionosphere; (2) the curvature of the earth; and (3) anisotropy caused by the geomagnetic field. That calculation requires the solution of nonlinear differential equations for as many as 10 to 20 modes. Each solution is subject to boundary conditions at the earth and ionosphere. That procedure uses substantial computer time, even on modern high-speed machines.

Despite their generality in other respects, however, those codes use equations that are valid only when the earth-ionosphere waveguide is uniform along the propagation path. Mixed paths are handled by dividing the waveguide into a number of laterally uniform segments, calculating properties of the full complement of modes in each segment, and then matching solutions at the segment boundaries. For example, analysis of a trans-Canadian path across six conductivity regions (see Fig. 1) would therefore require at least six times as much computer time as a path of equal length over seawater, even if

boundaries between regions were treated as abrupt. For more realistic
conductivity transitions, like that illustrated in Fig. 3, WAVEGUID
and WAVEPROP must divide each boundary into many uniform segments--the
so-called staircase fit to the actual transition. That process causes
a multifold increase in computer time.

To illustrate the above points, we use the WAVEPROP code to
calculate fields near transitions of varying abruptness. Figure 4
shows an example calculated for a transition from seawater (conduc-
tivity $\sigma = 4$ S/m) to Greenland ($\sigma = 10^{-5}$ S/m). The assumed frequency
is 45 kHz, which has a wavelength λ of 6.8 km and a reduced wavelength
$\lambda/2\pi$ of about 1 km.

The solid line (Fig. 4) is the electric field calculated for an
abrupt transition; the dashed line is the field when conductivity
changes linearly from 4 to 10^{-5} S/m over a distance of 1 km. The
signal for the abrupt transition is different from that for the 1 km-
wide transition, so it is necessary to account for finite boundary
widths.

The signal exhibits peaks and nulls behind the transition. That
structure is caused by interference among modes excited at the
shoreline; we had to retain 20 modes to calculate the interference
pattern accurately. To model the 1 km-wide transition, we had to
divide the boundary into about 30 segments, most of which were con-
centrated between conductivity values of 10^{-4} to 10^{-5} S/m. All 20
modes had to be calculated in each of the 30 boundary segments, so the
total calculation required 600 (20 $\times$ 30) numerical solutions of the
field equations.

Figure 4 highlights four problems that must be addressed in
constructing a computer model for atmospheric noise: (1) transitions
between geologically different regions must be accounted for where the
conductivity is low, (2) the signal depends on the width of the tran-
sition, (3) no data exist that define the correct transition widths in
most regions, and (4) full-fledged calculations for gentle boundaries
require an enormous number of numerical solutions. It is therefore
impractical to use WAVEGUID or WAVEPROP directly in an atmospheric
noise model that accounts for propagation across regions of both low
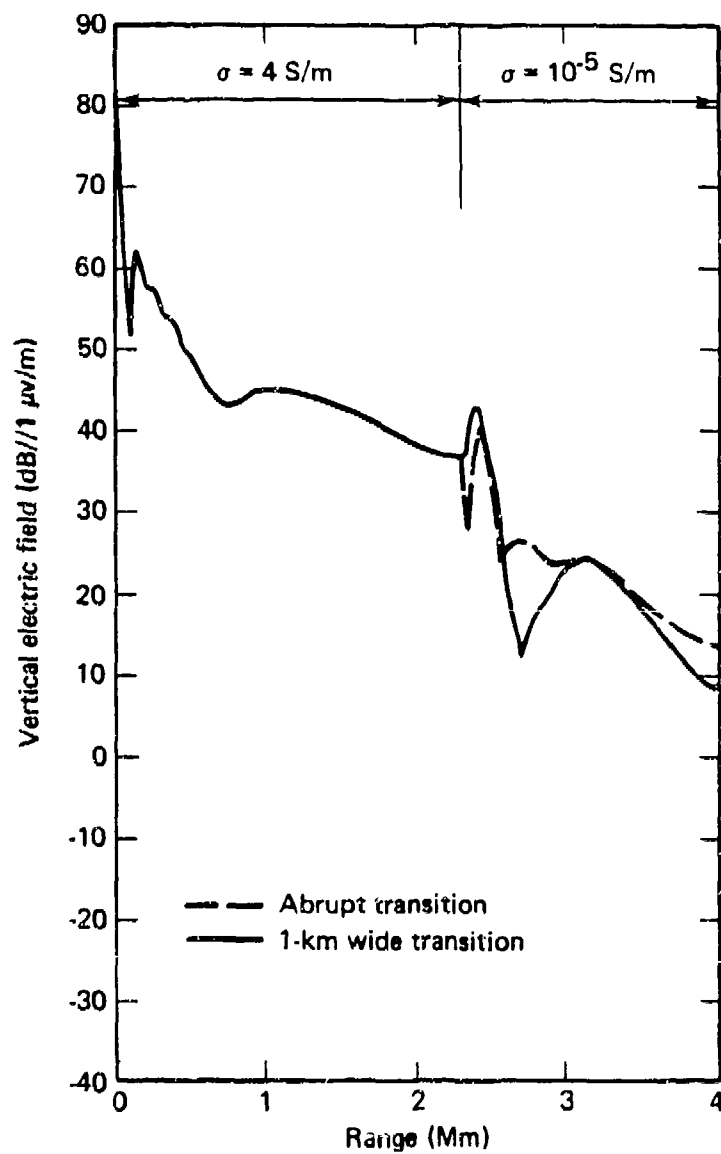and laterally nonuniform ground conductivity.

10

Figure 4. Effect of conductivity transition width on 45-kHz signal propagation over seawater and Greenland ice (power = 10 kW, aircraft altitude = 30,000 ft, antenna inclination = 10 deg to horizontal).

11

NEGLECT OF BACKWARD REFLECTIONS.

The well-known WKB, or slowly varying, approximation greatly simplifies propagation equations because, among other things, it permits us to neglect the signals reflected backward from gradients in the propagation medium. The WKB approximation can be applied when changes in the propagation medium occur over distances greater than the reduced wavelength $\lambda/2\pi$ (e.g., Budden [1985]). If changes occur over shorter distances, the transitions should be modeled as abrupt, and backward reflections should be included.

The wavelength λ lies between 5 and 20 km in the 15 to 60 kHz communications bands, so the reduced wavelength λ lies between 0.8 and 3 km--shorter than distances over which large-scale geophysical structures would be expected to change, and shorter than the lateral scales indicated, for example, by Fig. 3.* Those considerations lead to the intuitive conclusion that conductivity transitions are slow enough that reflections can be ignored, even near shorelines.

Mode coupling calculations require application of second-order formulas, details of which are given in the appendix. We use the gentleness of the conductivity transitions only to argue that backward reflections can be ignored. The appendix also estimates the coefficient of modal reflection R from the transition zone. For the TE modes, R is always small; for the TM modes, $|R| < 0.02$ in the VLF/LF range.

---

*Although nongradual transition might occur in the immediate vicinity of a shoreline, where the conductivity changes from 4 S/m (seawater) to a lesser--but still high--value characteristic of wet ground, the important transitions to low inland conductivities occur more slowly, as shown in Fig. 3.

SECTION 3

MODE-COUPLING EQUATIONS

In this section, we describe the model waveguide we use near conductivity boundaries and cite the connecting formulas based on that model. The appendix gives the derivations of those formulas.

PARALLEL-PLATE WAVEGUIDE MODEL OF TRANSITION ZONE.

The major complexity in the WAVEGUID/WAVEPROP class of codes is caused by the diffuse ionosphere, which requires that nonlinear differential equations for the height dependence of the wave admittance be solved numerically and iterated to match boundary conditions at the ground. Those matching conditions give the so-called modal equation, whose solution yields the attenuation rates and phase velocities of all waveguide modes.

That numerical complexity can be avoided by representing the true ionosphere by one that is uniform and sharply bounded. By properly selecting the effective ionospheric height h and conductivity σ_i, it is possible to define an equivalent, sharply bounded, earth-ionosphere waveguide that gives approximately the same VLF/LF propagation as the real waveguide [Wait, 1970].

The advantage of assuming a sharply bounded ionosphere is that the wave admittance is given by a simple formula, rather than by the numerical solution of a complicated differential equation. The modal equation is then a transcendental equation, easily solved without numerical integration. The disadvantage, of course, is that calculations made using a sharply bounded model waveguide are less precise than those made using a diffuse ionosphere.

The question is whether the computational ease of the sharply bounded model is worth the degraded precision. In most cases it is not. But, for the special problem of computing mode coupling at conductivity transitions, the precision loss is minor and acceptable. The reason is that the sharply bounded model need be used only to obtain connecting formulas that bridge each transition, which extends

over perhaps 10 to 20 km--an infinitesimal distance on a global scale. The WAVEGUID/WAVEPROP class of codes can be used on all other portions of the path.

Figure 5 is a schematic diagram of our model. Propagation is in the x-direction. The ground conductivity σ has a constant value of $\sigma = \sigma_{gI}$ at ranges shorter than $x = 0$ and a different constant value $\sigma = \sigma_{gII}$ at ranges greater than $x = \ell$. The transition from σ_{gI} to σ_{gII} occurs in the interval $0 < x < \ell$, where $\sigma = \sigma_g(x)$. The abrupt boundaries shown in Fig. 1, and used in most calculations, correspond to setting $\ell = 0$ in our model. The task in the present report is to derive formulas that connect fields at $x \leq 0$ to fields at $x \geq \ell$, subject only to the condition that $\sigma_g(x)$ varies slowly enough to permit us to neglect backward reflections.

Outside the region $0 < x < \ell$, we use full-wave codes of the WAVEGUID/WAVEPROP class, which account for the round earth and diffuse ionosphere but assume a uniform ground. The flat regions for $0 < x$ and $x > \ell$ indicate the region where we match the full-wave modes to the modes used in the parallel plate waveguide. In the diagram these appear to have a finite extent, but, in fact, we treat them in the calculations as if they were infinitesimally thin.

CONNECTING FORMULAS.

Tractable equations that describe mode coupling at a conductivity transition are derived in the appendix. Here, we present those equations and define certain parameters. We first write the equations in general notation, applicable to either polarization, and then specialize the notation to TM and TE modes. The equations given below omit the geomagnetic field and are valid for daytime or nuclear-disturbed ionospheres, but not for undisturbed nighttime ionospheres.

The refractive indices of the ionosphere and ground are:

$$n_i^2 = 1 - \frac{i\sigma_i}{\omega\epsilon_0} , \tag{1}$$

14
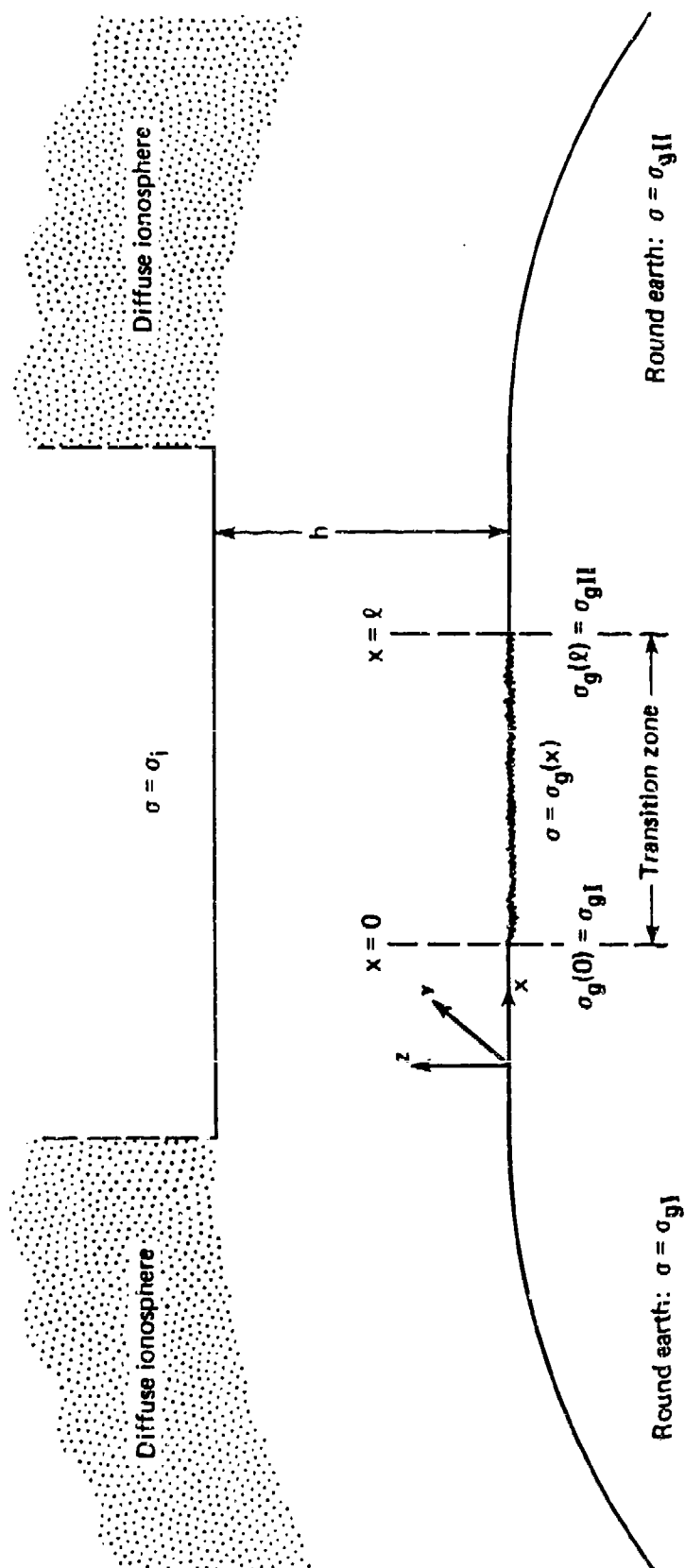
Figure 5. Parallel-plate waveguide model at conductivity transition.

and

$$n_g^2 = \epsilon_r - \frac{i\sigma_g}{\omega\epsilon_0} , \tag{2}$$

where ω is the angular frequency, ϵ_0 is the permittivity of free space, and ϵ_r is the relative permittivity of ground. Note that σ_g, ϵ_r, and hence n_g, are functions of x in the interval $0 \leq x \leq \ell$.

The solutions of the Booker quartic [Budden, 1985] in the iono-sphere and ground are:

$$q_{in}^2 = n_i^2 - 1 + C_n^2 , \tag{3}$$

and

$$q_{gn}^2 = n_g^2 - 1 + C_n^2 , \tag{4}$$

where C_n is the cosine of the eigenangle of the nth waveguide mode and is found by solving the modal equation, given below. To simplify the notation, we occasionally suppress the subscript n on q and C; those quantities, however, depend on the mode number.

Our goal is to express each waveguide mode beyond the transition $(x \geq \ell)$ in terms of the modes incident on the transition. For the nth incident mode, we write:

$$F_n^I(x, z) = \Gamma_n f_n(z) e^{-ikS_n^I x} \qquad (x \leq 0) , \tag{5}$$

where, k is the wave number and, depending on the polarization, F is the y-component of the magnetic or electric fields. In region I the ground conductivity is uniform, so the height-gain function $f(z)$ and the propagation coefficient S_n^I are independent of x. Both are functions of x in the region $0 \leq x \leq \ell$, because of the nonuniform

conductivity. The factor Γ_n (essentially the excitation factor of the nth mode in region I) is determined numerically using WAVEGUID/WAVEPROP solutions, which are presumed to be available for $x \leq 0$. The propagation coefficient is simply

$$s^2 = 1 - c^2 . \tag{6}$$

If we neglect backward reflections, the mode amplitude $F_n^{II}(\ell, z)$ on the far side of the transition is:

$$F_n^{II}(\ell, z) = \Gamma_n f_n(\ell, z) \sqrt{\frac{S_n(0)}{S_n(\ell)} \frac{\Lambda_n(0)}{\Lambda_n(\ell)}}$$

$$\times \left[1 + Q_n(\ell) \right] \exp \left[-ik \int_0^\ell S_n(x) \, dx \right] , \tag{7}$$

where Λ_n is a normalization function, and is given by Eq. (19) for TM and Eq. (27) for TE modes. Equation (7) is the sought-after connecting formula. We present and discuss the terms of that equation below.

The quantity Q_n is the mode-coupling factor, and, as shown by its formula, which is given below, accounts for energy scattered into the nth mode from other modes. It also accounts for energy scattered from the nth mode into other modes. Depending on the particular situation and the mode number, Q can therefore be either positive or negative. All terms other than Q in Eq. (7) involve only the nth mode, and account for changes in the propagation coefficient and height gain caused by the conductivity contrast between σ_{gII} and σ_{gI}.

The mode-coupling factor Q_n is the crux of the present report. It is given by:

$$Q_n = \sum_{i=1} Q_n^{(i)} , \tag{8}$$

17

where

$$Q_n^{(i)} = \sum_{\substack{m=1 \\ m \neq n}} \frac{\Gamma_m}{\Gamma_n} \sqrt{\frac{S_m(0)}{S_n(0)}} \, G_{nm}^{(i)} + G_{nn}^{(i+1)} \, , \qquad (9)$$

$$G_{nm}^{(i)}(x) = \sum_k \int_0^x g_{nk}(x') \, G_{km}^{(i-1)}(x') \, dx' \, , \qquad (10)$$

$$G_{nm}^{(1)}(x) = \int_0^x g_{nm}(x') \, dx' \, , \qquad (11)$$

and

$$g_{nm}(x) = \frac{1}{2\Lambda_n(x)} \sqrt{\frac{\Lambda_m(0) \, \Lambda_n(x)}{\Lambda_n(0) \, \Lambda_m(x)}} \left[\frac{S_n(x) + S_m(x)}{\sqrt{S_n(x) \, S_m(x)}} \right]$$

$$\times \left[\frac{\exp\left\{ -ik \int_0^x \left[S_m(x') - S_n(x') \right] dx' \right\}}{ik\left[C_m^2(x) - C_n^2(x) \right]} \right] \frac{d}{dx} \varsigma_n(x) \, ,$$

$$= 0 \quad \text{if } n = m \, . \qquad (12)$$

The sum over the index m in Eq. (9) accounts for scattering into the nth mode from all other modes. The term $G_{nn}^{(i+1)}$ accounts for scattering from the nth mode. In practice, it is seldom necessary to carry modes higher than m = 5. The sum over the index (i) in Eq. (8) accounts for various orders of scattering among modes. For example, the term $Q_n^{(1)}$ in Eq. (8) denotes single scattering, which involves only energy transferred directly between the nth and mth modes. The

term $Q_n^{(2)}$ denotes second-order scattering, in which energy is trans-
ferred from all modes into the $\underline{m}$th mode, and then from the $\underline{m}$th to the
$\underline{n}$th. The term $Q_n^{(3)}$ denotes third-order mode scattering, and so
forth. In practice, retaining only the single-scattering term $Q_n^{(1)}$ is
adequate for situations in which σ_{gI} and σ_{gII} exceed 10^{-3} S/m. Higher
order scattering terms must be retained for conductivities lower than
10^{-3} S/m, although in no case did we find it necessary to retain terms
beyond (i) = 4.

Note that g_{nm} in Eq. (12) is proportional to the term $d\zeta_n/dx$ [ζ_n
is defined in Eq. (20) for TM and Eq. (28) for TE] and is also propor-
tional to the lateral gradient of the ground conductivity. For
uniform ground, that derivative vanishes and there is no mode cou-
pling, because in that case $Q_n = 0$. Also, for uniform ground,
$S_n(\ell) = S_n(0)$, $f_n(\ell) = f_n(0)$, and $\Lambda_n(\ell) = \Lambda_n(0)$ in Eq. (7); so
$F_n^{II}(\ell) = F_n^{I}(0)$, as must be the case in the absence of conductivity
transitions.

Some terms in Eqs. (7) through (12) have different forms for TM
modes than for TE modes. Below, we give those forms for the two
polarizations.

TM Modes.

For TM modes, the amplitude F_n is given by:

$$F_n = Z_0 H_{ny} \, , \tag{13}$$

where $Z_0 = 377$ Ω and H_{ny} is the y-component of the $\underline{n}$th mode magnetic
intensity vector. The eigenangle cosines C_n are the solutions of the
TM modal equation:

$$iC\left(Z_i + Z_g\right) \cos kCh - \left(C^2 + Z_i Z_g\right) \sin kCh = 0 \, , \tag{14}$$

where the relative TM ionospheric and ground impedances are

$$Z_i = q_i/n_i^2 , \qquad (15)$$

and

$$Z_g = q_g/n_g^2 . \qquad (16)$$

In the transition region $0 \leq x \leq \ell$, the impedance Z_g, and hence C_n, is a function of x. For large conductivities ($\sigma_g \gtrsim 10^{-2}$), where $|Z_g| \ll 1$, the solutions to Eq. (14) are:

$$C_n \approx (n - 1/2) \frac{\pi}{kh} , \qquad n = 1, 2, \ldots \qquad (17)$$

The TM height-gain function is

$$f_n = \cos kCz + \frac{iZ_g}{C} \sin kCz . \qquad (18)$$

The normalizing function Λ_n is

$$\Lambda = \frac{1}{2ikC^2} \left\{ \left(C^2 - Z_g^2 \right) \left[ikh - \frac{1}{C^2 - Z_i^2} \left[Z_i - \frac{C}{q_i n_i^2} \right] \right] - Z_g \right\} . \qquad (19)$$

And the function ζ_n is simply

$$\zeta = Z_g . \qquad (20)$$

In the above equations, we have occasionally suppressed the x-dependence and the mode-number subscript n.

TE Modes.

For TE modes, the amplitude F_n is given by

$$F_n = E_{ny} ,\qquad (21)$$

where E_{ny} is the y-component of the <u>n</u>th mode electric vector. The eigenangle cosines C_n are solutions of the TE modal equation:

$$iC\left(Z_i + Z_g\right)\cos kCh - \left(1 + C^2 Z_i Z_g\right)\sin kCh = 0 ,\qquad (22)$$

where the TE relative ionospheric and ground impedances are

$$Z_i = 1/q_i ,\qquad (23)$$

and

$$Z_g = 1/q_g .\qquad (24)$$

For large conductivities, where $|Z_g| \ll 1$, the solution to Eq. (22) is:

$$C_n \approx \frac{n\pi}{kh} ,\qquad n = 1, 2, \ldots .\qquad (25)$$

The TE height-gain function is

$$f_n = \cos kCz + \frac{iq_g}{C}\sin kCz .\qquad (26)$$

The normalizing function Λ_n is

$$\Lambda = \frac{1}{2ik}\left\{\left[1 - \left(\frac{q_g}{C}\right)^2\right](ikh + Z_i) - q_g/C^2\right\} .\qquad (27)$$

21

And the function ζ_n is

$$\zeta = q_g .$$ (28)

DETERMINATION OF WAVEGUIDE HEIGHT h AND IONOSPHERIC CONDUCTIVITY σ_i FROM WAVEGUID/WAVEPROP SOLUTIONS.

A major benefit of the localized parallel-plate-waveguide approach is that it permits the eigenangle cosines to be found from Eqs. (14) and (22), the simple modal equations. The WAVEGUID/WAVEPROP codes, on the other hand, must solve nonlinear differential equations and iteratively match boundary conditions to find C_n. The latter procedure requires much computer time and may be labor-intensive for even a skilled operator. The task remains, however, to find a combination of effective waveguide height h and ionospheric conductivity σ_i that gives values of C_n that are nearly the same as those obtained using WAVEGUID/WAVEPROP in conjunction with realistic diffuse ionospheres.

The starting point for finding h and σ_i is the series of values of C_n calculated with WAVEGUID/WAVEPROP in region I ($x < 0$--see Fig. 5). By using either the equation for TM [Eq. (17)] or for TE [Eq. (25)], we can write:

$$h_n \approx \frac{\lambda}{2\left(C_{n+1} - C_n\right)} .$$ (29)

Strictly speaking, the value of h_n given by Eq. (29) depends on the mode number n, but, in practice, h varies only slightly with n (in our experience, variation of h is less than 5 percent. We therefore use

$$h = \frac{1}{N} \sum_{n=1}^{N} h_n ,$$ (30)

where N is typically a number on the order of 5.

22

After finding h, we then use the mode equations [Eqs. (14) and (22)] to find σ_i. Specifically, we insert C_n (from WAVEGUID/ WAVEPROP), Z_g, and h into those equations and solve for Z_i, which defines the value of σ_i. As the case for h, the values of σ_i calculated in that manner depend only slightly on mode number n, so we use a value averaged over the important modes.

TEST CASES

In this section, we present sample calculations that test the approximate formulas of Sec. 3 against exact ones made with the WAVEPROP code. We also discuss practical aspects of applying those formulas.

PARALLEL-PLATE WAVEGUIDE.

Figure 6 illustrates how closely the parallel-plate model waveguide approximates the actual waveguide. It shows ReC_n versus ground conductivity for a frequency of 45 kHz and the five lowest order TM modes. The values of C_n (denoted by dots in the figure) were calculated numerically using WAVEPROP and account for earth curvature, the diffuse height-profile of the ionosphere, and the geomagnetic field. We assume north-south daytime propagation and a 60 deg geomagnetic dip angle.

To define the equivalent height and conductivity of the parallel-plate waveguide, we insert $\sigma_g = 10^{-2}$ S/m and the corresponding C_n values from Fig. 6 into Eqs. (14), (29), and (30) to find h = 59 km and $\sigma_1 \sim 10^{-4}$ S/m. Substituting those values of h and σ_1 back into Eq. (14) gives the values of ReC_n indicated by the solid lines in Fig. 6.

The agreement between the "exact" (WAVEPROP) and approximate (parallel-plate waveguide) results is excellent for all five modes and the entire range of ground conductivities.* It would be even closer for frequencies lower than 45 kHz, which are less affected by the

---

*The first mode at 10^{-2} S/m is the only one in error by a substantial amount. This mode is the most oblique; we expect it to be affected the most by the curvature of the earth, which we ignore. That mode is typically not as important as the second, since it has higher attenuation and lower excitation. Moreover, at high conductivity ($\sigma_g > 10^{-3}$ S/m) there is very little mode coupling, so the error indicated does not matter for our analysis. However, this mode is the Brewster's mode (i.e., $C \approx Z_g$) for $\sigma_g < 10^{-3}$ S/m, where mode coupling is important. In this region the modes match very well.
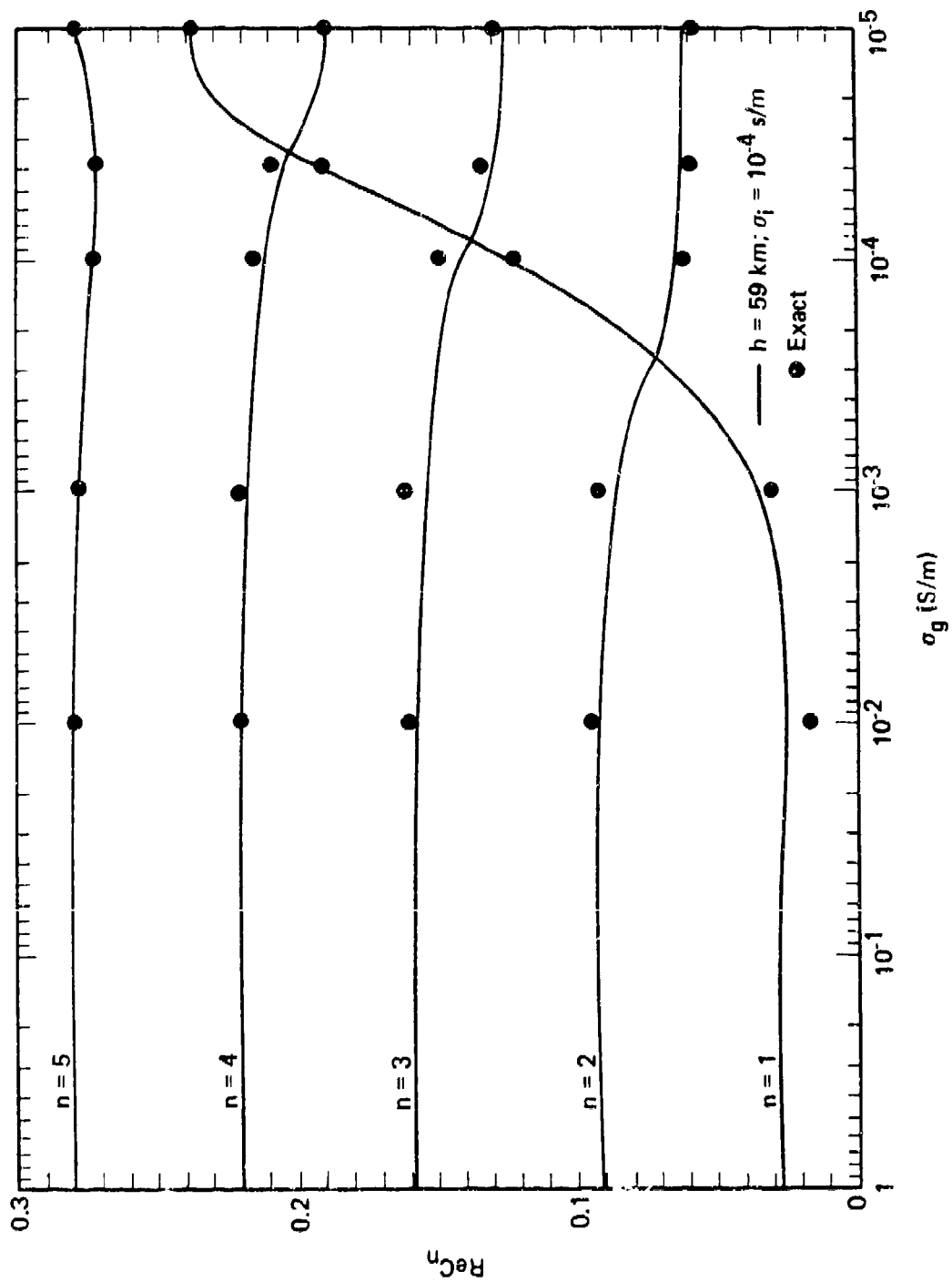
Figure 6. Eigenangles of first five TM modes: comparison of exact values with values from parallel-plate waveguide ($F = 45$ kHz).

earth's sphericity and less sensitive to waveguide parameters. Calculations (not reproduced here) show equally close agreement for TE modes. The modal equations [Eqs. (14) and (22)] may therefore be used to find $C_n(x)$ across the conductivity transition. That simplification reduces computer running time enormously. [Note that although Eqs. (14) and (22) give accurate values of $|C_n| \approx ReC_n$, they do not provide accurate values of ImC_n, which govern the waveguide attenuation rates. Because $ImC_n \ll ReC_n$, and because the assumed transition zones are too narrow ($\ell \ll 100$ km) for attenuation to be important, that inaccuracy causes no problems for the application addressed in the present report. However, the parallel-plate model waveguide cannot be used to approximate long (> 100 km) path segments where attenuation is important and must be calculated accurately.]

MODE COUPLING.

To examine the dependence of mode coupling on the conductivities σ_{gI} and σ_{gII}, we assume a conductivity transition where $\sigma_g(x)$ varies according to the formula

$$\log_{10} \sigma_g(x) = -5x/\ell \ . \tag{31}$$

If we use this logarithmic variation, the results depend only on σ_{gII}, not on the scale length ℓ. In this case, it is true that mode coupling depends only on the endpoint values σ_{gI} and σ_{gII}.

If nonlogarithmic transitions are used, the mode coupling depends on transition shape as well as on the endpoint values. That dependence is slight, however, and to a first approximation it can usually be ignored. Mode coupling at a boundary can therefore be calculated by specifying σ_{gI} and σ_{gII} and using any convenient model for $\sigma_g(x)$ in the zone $0 \le x \le \ell$, provided that the transition is gentle enough so that reflections can be ignored. As previously mentioned, that near-independence of mode coupling on transition shape is important, because there are virtually no data on how σ_g varies within transition zones.

To illustrate how mode coupling depends on the conductivity contrast at a boundary, we assume a second-order (n = 2) TM mode of

26

unit amplitude incident on a transition zone where the conductivity changes from $\sigma_{gI} = 1$ S/m to values of σ_{gII} that range from 1 to 10^{-5} S/m. No other modes are present for $x < 0$, so

$$\Gamma_n = \begin{cases} 1 & \text{for } n = 2 , \\ 0 & \text{for } n \neq 2 , \end{cases} \qquad (32)$$

in Eq. (5). We further assume a frequency of 30 kHz.

Figure 7a shows the amplitude of mode 2 versus σ_{gII}, and Figs. 7b-e show the ground-level amplitudes of modes 1, 3, 4, and 5, respectively. For ease of comparison, the scales used in Figs. 7a-e are consistent. Each figure shows plots of several graphs corresponding to the various orders of coupling (values of the index i) discussed above in conjunction with Eqs. (8) and (9).

Figures 7a-e show that when σ_{gII} exceeds about 3×10^{-3} S/m, the amplitude of the second mode remains near unity and the amplitudes of the other modes are small. For values of σ_{gII} below 3×10^{-3} S/m, however, the amplitudes of modes 1, 3, 4, and 5 increase at the expense of mode 2. That behavior confirms our earlier assertion that mode coupling is weak for high ground conductivities, but can be strong for low conductivities.

Another conclusion to be drawn from Figs. 7a-e is that retention of only first-order coupling (i = 1) usually provides accurate results, although it is necessary to retain as many as three or four orders at the lowest values of σ_{gII}. In no case do we find that orders higher than i = 4 contribute significantly.

GENTLE VERSUS ABRUPT BOUNDARIES.

In our final example, we compare mode coupling across gentle boundaries to mode coupling across abrupt boundaries, such as those indicated in Fig. 1. We make that comparison because, as discussed in Sec. 2, mixed-path calculations usually assume abrupt boundaries; and, notwithstanding the fact that the WKB approximation is invalid for
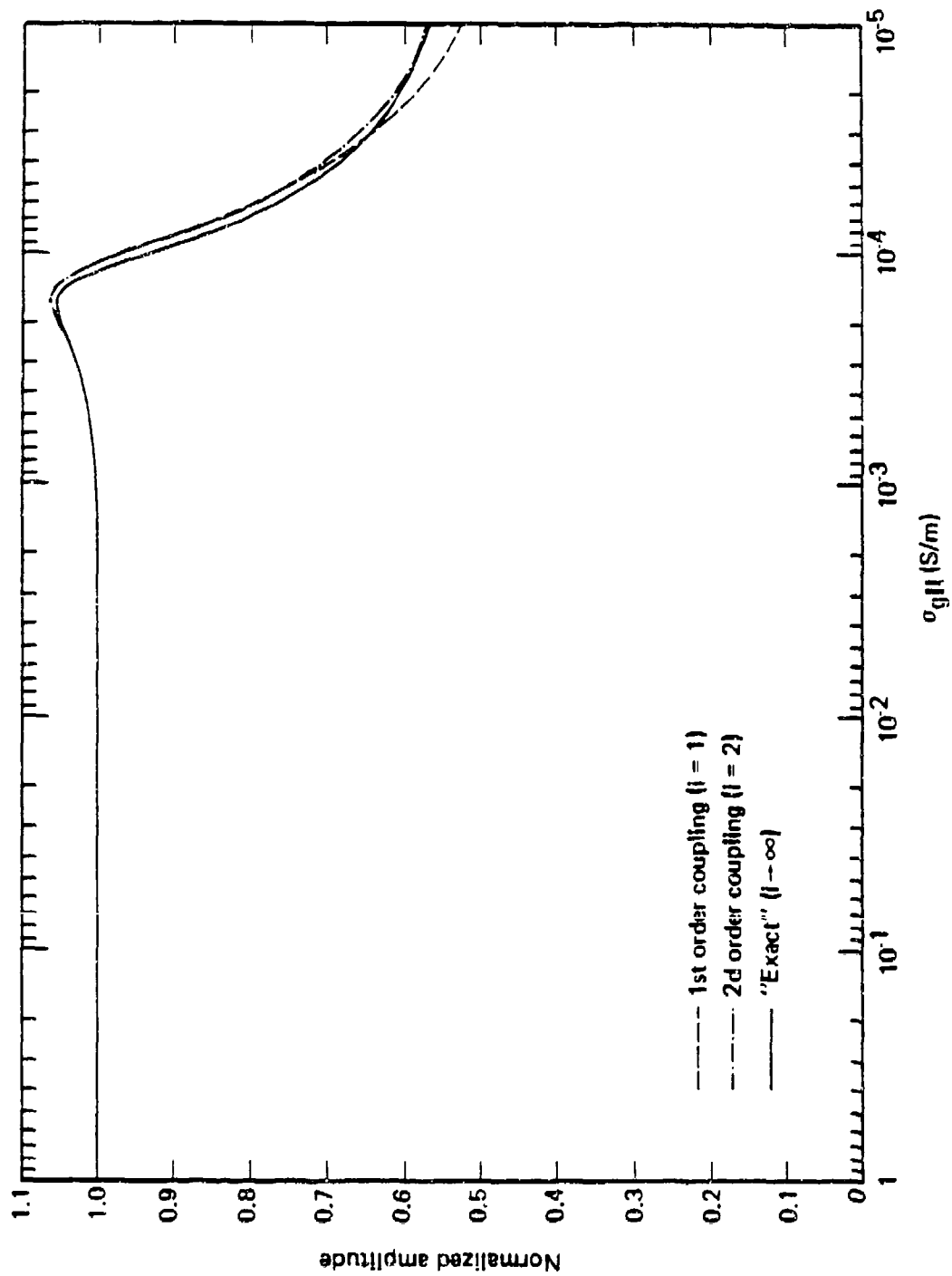
Figure 7. Amplitude of TM mode across gentle conductivity transition (F = 30 kHz).

a. Second mode (n = 2).

Normalized amplitude

$\sigma_{g||}$ (S/m)

——— 1st order coupling (l = 1)
—·—·— 2d order coupling (l = 2)
——— "Exact" (l → ∞)
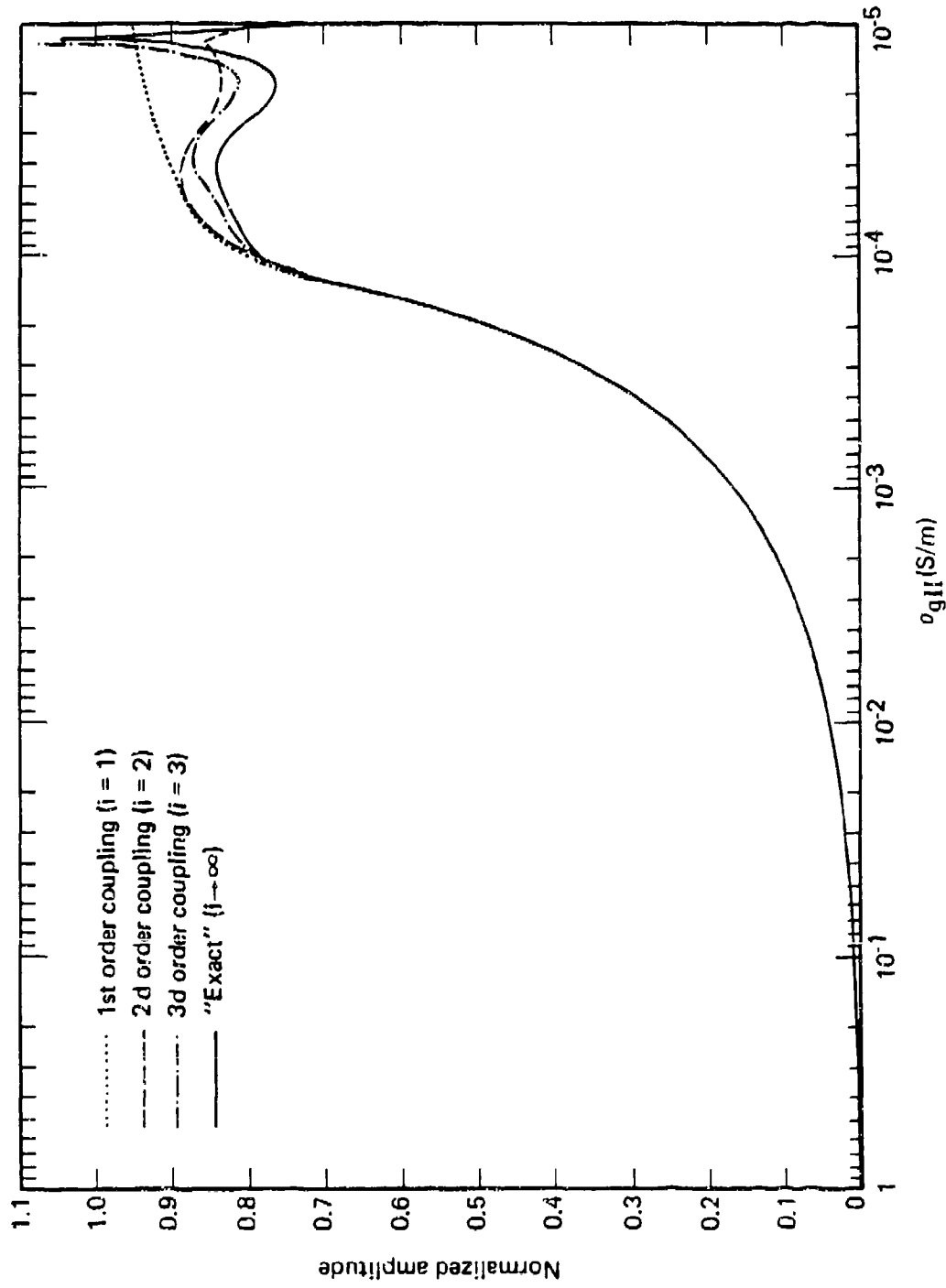
b. First mode (n = 1).

Figure 7. Amplitude of TM mode across gentle conductivity transition (F = 30 kHz) (Continued).

29
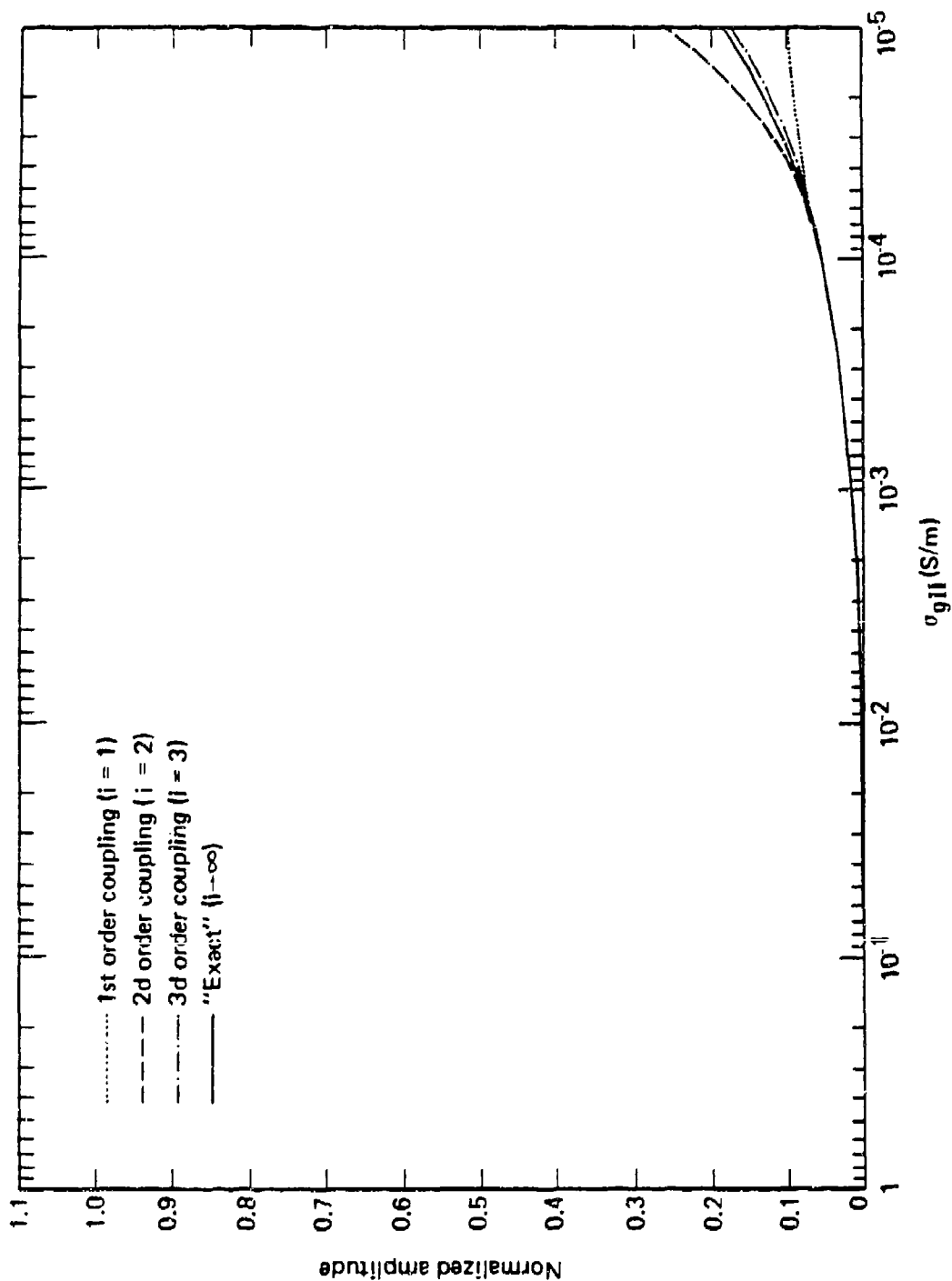
c. Third mode (n = 3).

Figure 7. Amplitude of TM mode across gentle conductivity transition (F = 30 kHz) (Continued).

Legend (within figure):
.... 1st order coupling (i = 1)
- - - - 2d order coupling (i = 2)
- · - · - 3d order coupling (i = 3)
——— "Exact" (i→∞)

Axes: Normalized amplitude (vertical); σ_{g11} (S/m) (horizontal)

30

Legend (chart):
.... 1st order coupling (i = 1)
– – – 2d order coupling (i = 2)
–·–·– 3d order coupling (i = 3)
——— "Exact" (i→∞)

Normalized amplitude

σ_{gII} (S/m)

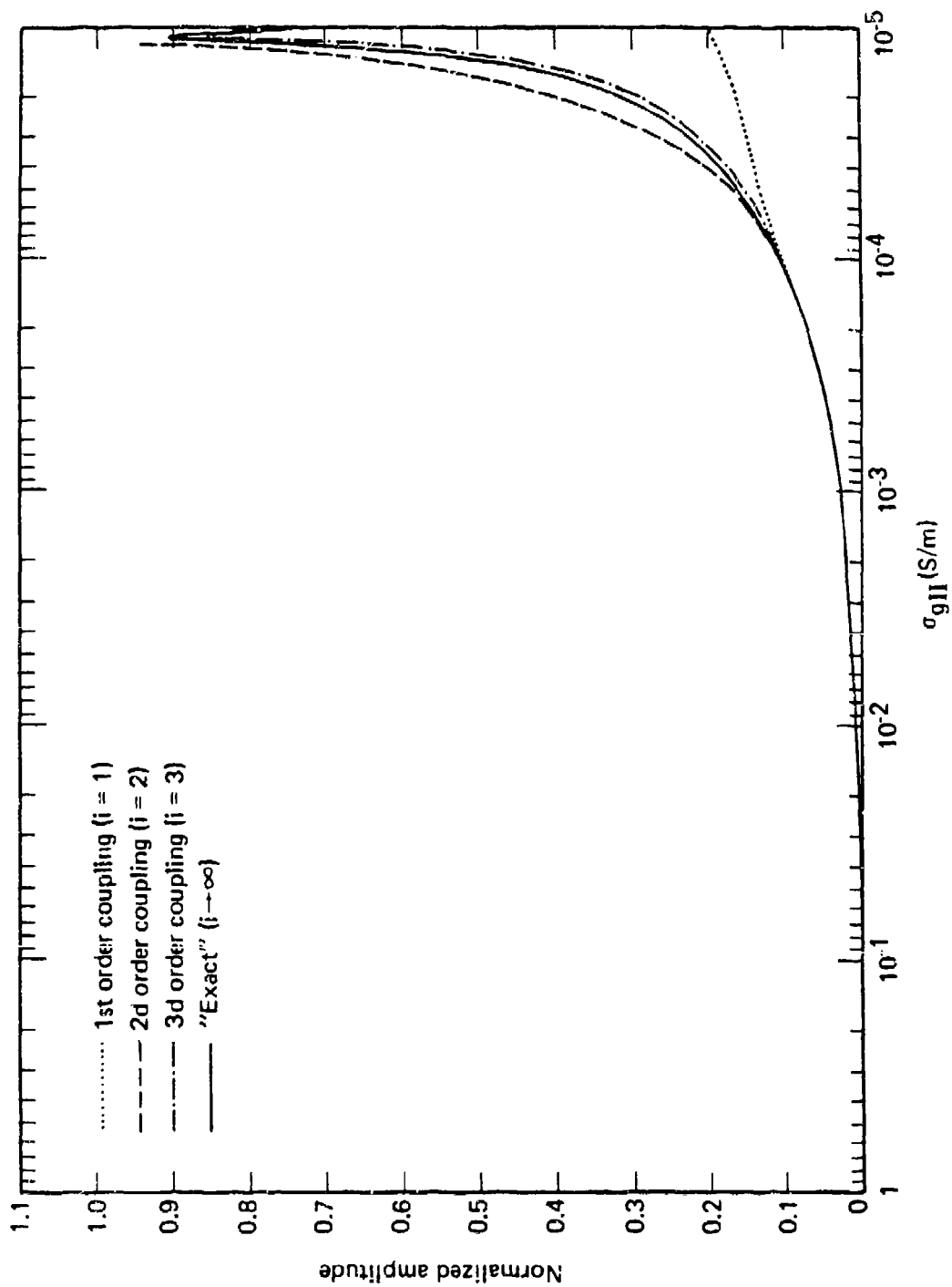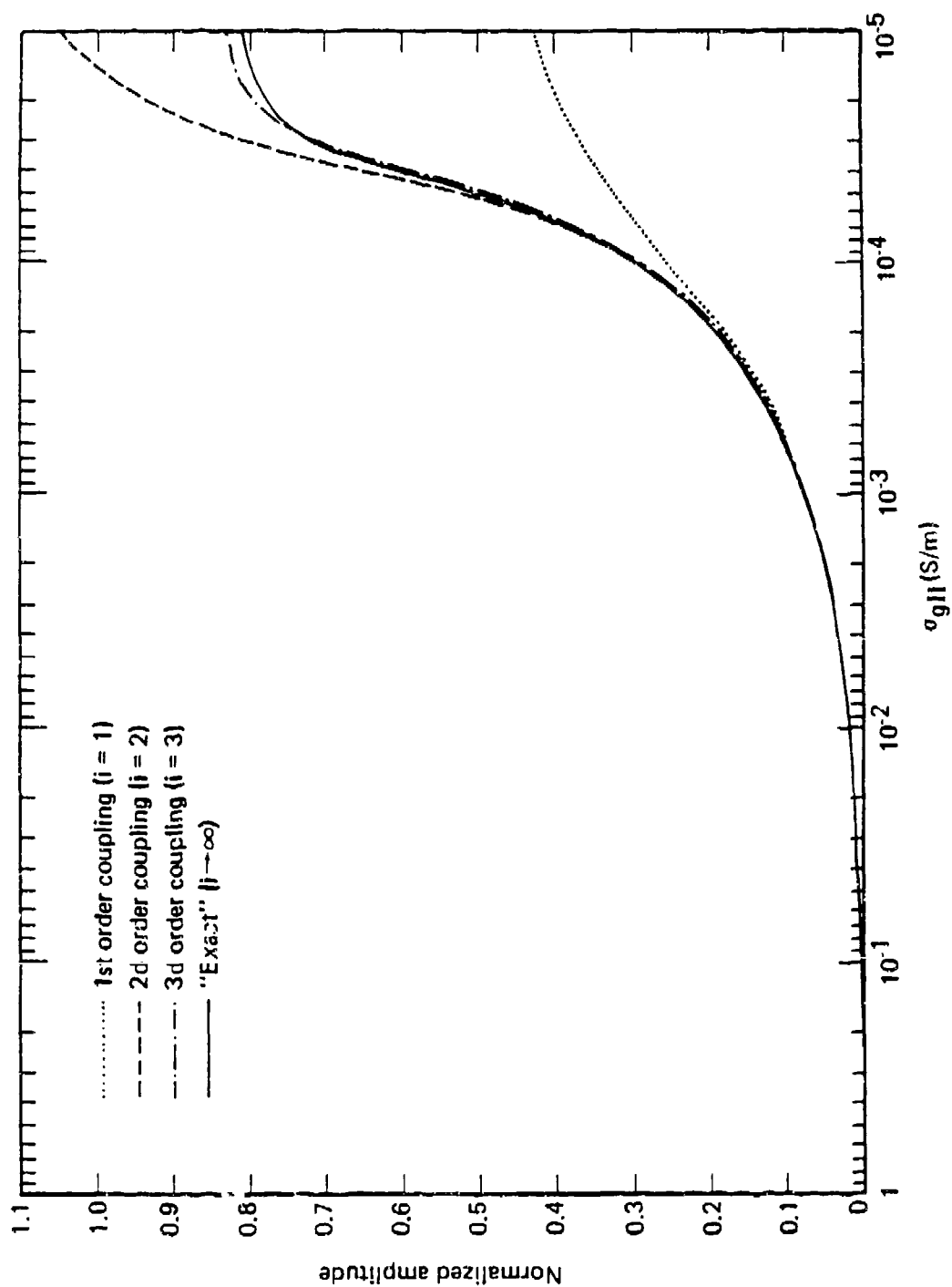d. Fourth mode (n = 4).

Figure 7. Amplitude of TM mode across gentle conductivity transition (F = 30 kHz). (Continued).

31

Figure 7. Amplitude of TM mode across gentle conductivity transition (F = 30 kHz) (Concluded).

e. Fifth mode (n = 5).

abrupt boundaries, the WAVEGUID/WAVEPROP codes omit backward-scattered modes for computational convenience.

The formulas for the gentle boundary are presented and discussed in Sec. 3. For an abrupt boundary, where $\ell = 0$, we have:

$$\Gamma_n^+ \approx \frac{1}{2iks_n^+\Lambda_n^+} + \sum_{m=1}^{\infty} \Gamma_m^- \frac{Z_g^+ - Z_g^-}{S_n^+ - S_m^-} , \qquad (33)$$

where the superscripted plus (+) and minus (-) denote, respectively, parameters in regions I and II. Backward reflections are also omitted from Eq. (33). This is consistent with WAVEGUID and WAVEPROP.[*]

We again assume that $\sigma_{gI} = 1$ and only a second-order incident mode:

$$\Gamma_n^- = \begin{cases} 1 & \text{if } n = 2 , \\ 0 & \text{if } n \neq 2 , \end{cases} \qquad (34)$$

but here we use a frequency of 45 kHz, in order to give us a better test of the method. Figure 8 plots, as a function of σ_{gII}, the lowest five TM mode amplitudes at the beginning of region II, i.e., where $x = 0^+$.

The results for the abrupt and gentle cases are about the same if $\sigma_{gII} > 10^{-3}$ S/m, again confirming that almost any model will give good results if the ground conductivity is high enough. However, for $\sigma_{gII} < 10^{-4}$ S/m, the differences between the two boundary types are substantial. The first (n = 1) mode is the so-called Brewster mode which, although strongly excited, is very heavily attenuated over poorly conducting ground. At great distances beyond the boundary, the second (and least attenuated) mode is the most important. Figure 8

---

[*]In the sum of Eq. (33), $Z_g^+ \longrightarrow Z_g^-$, L'Hospital's rule gives, for the m = n term,

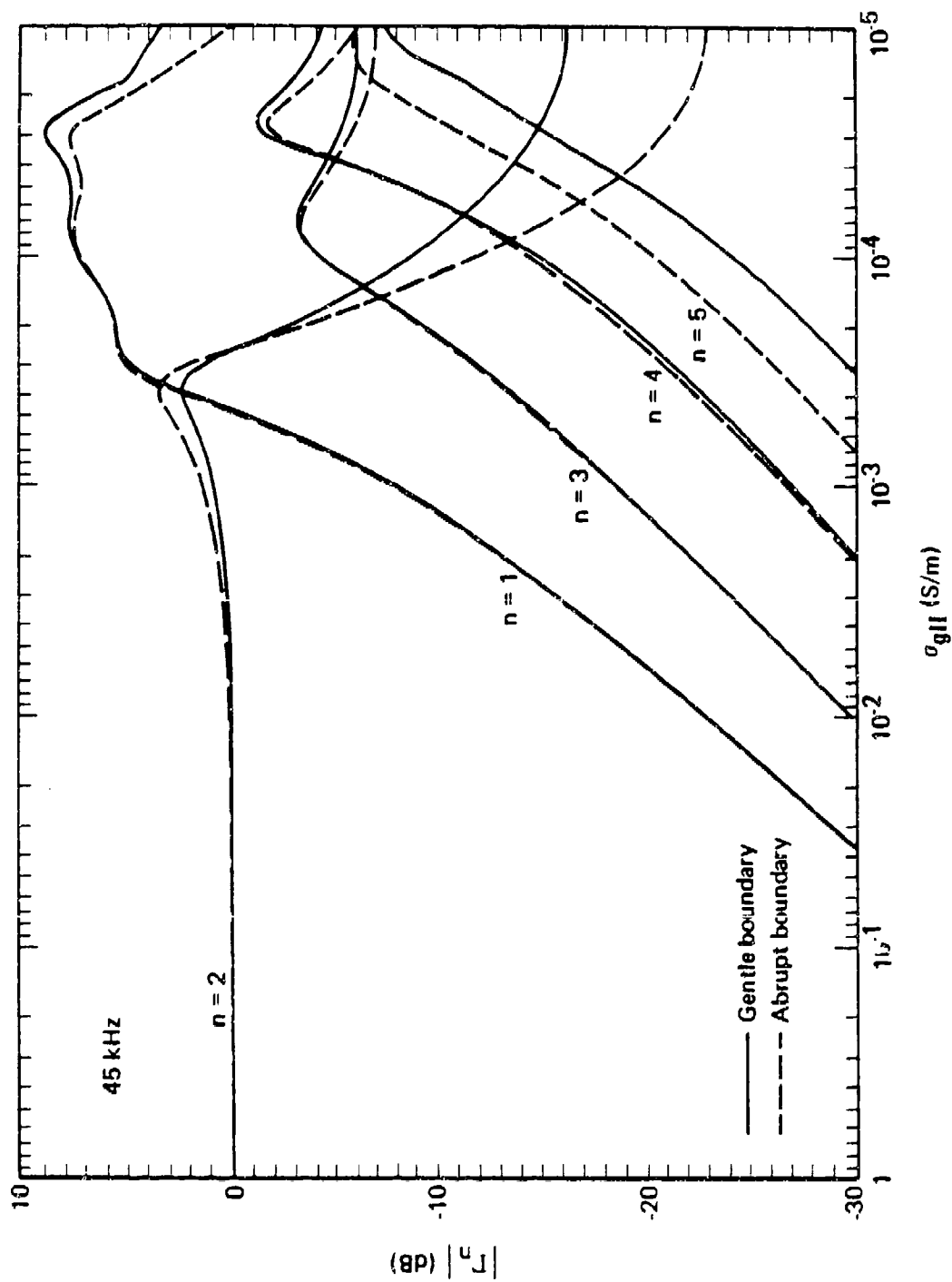$$\frac{\Lambda_n^-}{\Lambda_n^+} \frac{S_n^-}{S_n^+} \Gamma_n^- .$$

Figure 8. Amplitudes of first five TM modes at beginning of region II: comparison of gentle and abrupt boundaries (F = 45 kHz).

34

shows that, for $\sigma_{\text{gII}} < 10^{-4}$ S/m, the abrupt and gentle models give mode-2 amplitudes that disagree by 6 dB. As discussed in Sec. 2, we believe the gentle boundary to be more realistic than the abrupt.

SECTION 5
CONCLUSIONS

In this report, we have derived formulas for approximating VLF/LF waveguide-mode amplitudes beyond a conductivity boundary in terms of the mode-amplitudes incident on that boundary. Although algebraically complicated, those formulas are easily programmed and require far less computer running time than numerical mode-coupling algorithms used in "exact" computer codes, such as WAVEGUID/WAVEPROP. The formulas have two desirable features: they are computationally simple and they depend mainly on the ground conductivity values on either side of a transition, but only slightly on the conductivity variation within the transition itself. Data from available maps of worldwide ground conductivity can therefore be inserted directly into the formulas.

The mode-coupling formulas are subjected to three areas of approximation, which we believe are valid under most circumstances encountered in practice. First, and most important, we substitute an equivalent parallel-plate waveguide for the actual waveguide in the short spatial interval that contains the transition zone. Second, we ignore reflections from that zone, which requires that all conductivity changes within the transition zone be gradual (occurring over distances at least as long as the reduced wavelength $\lambda/2\pi$). Third, we neglect phase and use only the magnitudes of the modes when performing mode sums. However, the mode-coupling equations [Eqs. (7-12)] are derived complete with phase terms that can, at the discretion of the analyst, be retained.

The latter approximation--neglect of phase--is appropriate for models of worldwide noise because such models divide the earth into a large number of sections that behave as equivalent noise transmitters. Each noise transmitter contains many lightning sources that are uncorrelated and noncoherent. Moreover, noise models involve average rather than instantaneous values, and such averages smear out the nulls that occur on signals from coherent transmitters. The main effect of phase in the mode sum is to create nulls; and accurate

calculation of field strength in a null requires retention of many modes. Neglect of phase in the mode sum--but not elsewhere-- eliminates nulls and thus substantially reduces the required number of modes.

Although derived for inclusion in future computer models of VLF/LF worldwide atmospheric noise, the mode-coupling formulas can be used in any application where the number of propagation paths is so large that the computer running time becomes a problem. However, when the formulas are used to describe coherent signals rather than noise, the phase terms must be retained. Moreover, because retention of phase necessitates inclusion of more higher order modes, and because the effective height h depends somewhat on mode number n, the mode-specific h_n [Eq. (29)] should be used instead of the average h [Eq. (30)].

SECTION 6
LIST OF REFERENCES

Bostick, F. X., H. W. Smith, and J. E. Boehl, *Magnetotelluric and DC Dipole-Dipole Resistivity Measurements in the Northern Olympic Peninsula,* University of Texas, Electrical Geophysical Laboratory, Austin, Texas, May 1977.

Budden, K. G., *The Progapation of Radio Waves,* Chap. 7, Cambridge University Press, New York City, 1985.

Field, E. C., et al., *Effects of Antenna Elevation and Inclination on VLF/LF Signal Structure,* Air Force Systems Command, Rome Air Development Center, Griffiss Air Force Base, New York, RADC-TR-76-C-37S, December 1976.

Kraichman, M. B., *Handbook of Electromagnetic Propagation in Conducting Media,* U.S. Naval Ordnance Laboratory, Silver Spring, Maryland, U.S. Government Printing Office, Washington, DC, 1970.

Pappert, R. A., and L. R. Shockey, *Mode Conversion Program for an Inhomogeneous Anisotropic Ionosphere,* Naval Ocean Systems Center, San Diego, California, Interim Report 722, May 1972.

Pappert, R. A., W. F. Moler, and L. R. Shockey, *A Fortran Program for Waveguide Propagation which Allows for Both Vertical and Horizontal Dipole Excitation,* Defense Nuclear Agency, Washington, DC, Interim Report 702, June 1970.

Wait, J. R., *Electromagnetic Waves in Stratified Media,* Pergamon Press, Inc., Elmsford, New York, 1970.

Westinghouse Electric Corporation, *Worldwide VLF Effective Conductivity Map,* Report 80133F-1, January 1968.

APPENDIX
DERIVATION OF EQUATIONS

INTRODUCTION.

This appendix derives our method for efficiently calculating the coupling of modes across a region of changing ground conductivity. We assume that the earth and ionosphere can be modeled locally as a parallel-plate waveguide. That assumption leads to equations for the propagation constant, which can be quickly solved numerically in the case of the TM modes and analytically in the case of TE modes. In that way, we avoid the complicated mode-coupling calculations used by the more precise WAVEPROP program. Here, we restrict our attention to normal daytime ionospheric conditions, but the method can, in principle, be extended to nighttime conditions.

We use a generalized version of the method developed by Wentzel, Kramers, and Brillouin for quantum mechanical applications--hence the name WKB method. In essence, they replaced the search for a wave-equation solution, which is a rapidly varying function, by a search for a more slowly varying function. Under certain conditions-- typically, when the medium is changing slowly over a wavelength--the slowly varying function can be assumed to be a constant. That is known as the WKB approximation--or, stated more precisely--the first-order WKB approximation. We do not make this assumption, however, but find a coupled set of exact differential equations for this more slowly varying function. Thus, our method could be called a generalized WKB method. If we account for both mode coupling and backward mode reflection from the boundary, the equations are far too complex to be solved quickly. Therefore, we make the WKB-like assumption that the change in the ground conductivity is slow enough that backward reflections can be ignored. At the end of this appendix we test that assumption by making the opposite assumption--that mode coupling can be ignored--and find that the reflection is very small.

We use Budden's renormalization of the magnetic field (see Budden [1985]). Thus the field H used in this appendix is, in fact, the

magnetic field multiplied by the impedance of free space. The wave impedances are therefore dimensionless and should be multiplied by 377 Ω to put them into MKS units. The above also removes the distinction between the magnetic and electric fields. In this appendix, we often combine the standard TE (E_y, H_x, H_z) or TM field components (H_y, E_x, E_z) into a new field called $\vec{F}$. That notation allows us to derive one set of equations that is applicable to both TE and TM modes.

We also assume that the impedance of the earth is independent of the mode parameter (C_n). As shown later, that approximation is tantamount to assuming q_g is independent of C_n. The definition of q_g is

$$q_g = \left[n_g^2 - 1 + C_n^2 \right]^{1/2} \approx \left[n_g^2 - 1 \right]^{1/2} \left[1 + \frac{1}{2} \frac{C_n^2}{n_g^2 - 1} \right] . \qquad (35)$$

The mode dependence is second order in C_n/n_g. If we make the restriction that $|C_n| \leq 0.5$, then the largest error is at very low conductivity ($\sigma_g \sim 10^{-5}$ S/m), where it is about 2 percent. That approximation is not critical to the analysis, but allows analytic forms to be derived for the TE case. Without that approximation, integrals over height from 0 to ∞, would have to be changed to integrals from $-\infty$ to ∞, and some other analytic forms will change.

Many quantities used here are functions of distance from the transmitter (denoted by x), height above the ground (z), and mode number (n). When it does not cause confusion, we omit the function parameters or mode number subscript in order to avoid visual complexity.

MODEL.

We treat the earth as a conducting half-space below z = 0, and the ionosphere as a conducting half-space above z = h. The index of refraction for the earth and the ionosphere is, respectively,

$$n_g^2 = \epsilon_r - i \frac{\sigma_g}{\omega \epsilon_0} , \qquad (36a)$$

$$n_i^2 = 1 - i \, \frac{\sigma_i}{\omega \epsilon_0} \, . \tag{36b}$$

Here, we assume that $\sigma_g \geq 10^{-5}$ S/m, but we make no assumption (momentarily) about σ_i. We also assume that the conductivity of the earth is constant for $x \leq 0$ and $x \geq \ell$, but that it changes in the region $0 < x < \ell$. For our purpose, the conductivity is considered to be continuous. We assume that the boundary is far enough from the transmitter that the total field is made up of a sum of fields of individual waveguide modes. For example, the electric field is

$$E_y = \sum_n E_{yn} \, . \tag{37}$$

MAXWELL'S EQUATIONS.

By using Budden's renormalization we can show that Maxwell's equations for the TE case become:

$$H_x = \frac{1}{ik} \frac{\partial E_y}{\partial z} \, , \tag{38}$$

$$H_z = - \frac{1}{ik} \frac{\partial E_y}{\partial x} \, , \tag{39}$$

and

$$\left[ikn^2(x) - \frac{1}{ik} \frac{\partial^2}{\partial z^2} \right] E_y + \frac{\partial}{\partial x} H_z = 0 \, . \tag{40}$$

For the TM case, Maxwell's equations become:

$$ikn^2 E_x = - \frac{\partial H_y}{\partial z} \, , \tag{41}$$

41

$$ikn^2 E_z = \frac{\partial H_y}{\partial x} \quad , \tag{42}$$

and

$$-ikH_y + \frac{1}{ikn^2} \frac{\partial^2 H_y}{\partial z^2} + \frac{\partial E_z}{\partial x} = 0 \quad . \tag{43}$$

FIELDS WHEN σ_g CHANGES.

To illustrate our technique, we use F_y, the y component of the field, in the region where ground conductivity is not changing, i.e., $x < 0$. (Note that $F_y = E_y$ in the TE case and $F_y = H_y$ in the TM.) The form of F_y is well known; i.e.,

$$F_y = \sum_n f_n(z) \left[\Gamma_n e^{-ikSx} + R_n e^{ikSx} \right] \quad . \tag{44}$$

Here $f_n(z)$ is the height gain function, $\Gamma_n e^{-ikSx}$ represents the forward-moving wave, and $R_n e^{ikSx}$ represents the backward-moving wave, i.e., that part of the wave reflected from the boundary. We normalize the height gain to one on the ground, so that the excitation (Γ_n) and reflection (R_n) factors represent the forward and backward field on the ground at $x = 0$.

In the region where the ground conductivity is changing we need a form that reduces to Eq. (44). Thus, for $x \geq 0$,

$$F_y = \sum_{n=1}^{\infty} f_n(z, x) \left[A_n(x) + B_n(x) \right] \quad . \tag{45}$$

Here, $A_n(x)$ represents the forward-moving wave, $B_n(x)$ represents the backward-moving wave, and $f_n(z, x)$ is the height gain, which is dependent on x. Here, A_n and B_n are arbitrary functions of x. We place restrictions on the height gain term f_n, and determine what form $A_n(x)$ and $B_n(x)$ must have to satisfy Maxwell's equations.

42

The restriction on f_n is that locally it must satisfy the wave equation

$$\left[\frac{\partial^2}{\partial z^2} + k^2 q^2(x, z) \right] f_n(z, x) = 0 , \qquad (46)$$

where $q^2 = n^2(x, z) - 1 + C_n^2$.

We discuss the height-gain term f_n in more detail below; there we show that f_n is orthogonal in the sense that

$$\int_0^\infty f_n(z, x) f_m(z, x) dz = \Lambda_n(x) \delta_{nm} . \qquad (47)$$

The boundary conditions satisfied by f_n determine the modal equation that gives the value of C_n. Thus, the information about the ground conductivity is contained in f_n, so we can restrict ourselves to the region within the waveguide ($0 \le z \le h$).

Equations (39) and (42) can be written:

$$F_z = - \frac{1}{ik} \frac{\partial}{\partial x} F_y . \qquad (48)$$

(So $F_z = H_z$ in the TE case and $F_z = -E_z$ in the TM case.) The form of F_z that is consistent with Eq. (45) and that reduces to the correct form for $x \le 0$ is

$$F_z = \sum_{n=1}^\infty f_n S_n \left(A_n - B_n \right) . \qquad (49)$$

We combine Eqs. (40) and (43) (in the waveguide) to give:

$$\left(ik - \frac{1}{ik} \frac{\partial^2}{\partial z^2} \right) F_y = - \frac{\partial}{\partial x} F_z . \qquad (50)$$

The functions $A_n(x)$ and $B_n(x)$ must satisfy Eqs. (48) and (50). To find out what this requires of $A_n(x)$ and $B_n(x)$, we use Eqs. (45) and (49), along with Eq. (46) and the orthogonality of f_n to derive the following after some algebra. (Here, a prime symbol denotes the differentiation with respect to x.)

$$A_n' + B_n' + ikS_n\left(A_n - B_n\right) + \sum_{m=1}^{\infty} K_{mn}\left(A_m + B_m\right) = 0 \ , \qquad (51)$$

$$A_n' - B_n' + ikS_n\left(A_n + B_n\right) + \frac{S_n'}{S_n}\left(A_n - B_n\right) + \sum_{m=1}^{\infty} K_{mn}\left(A_m - B_m\right)\frac{S_m}{S_n} = 0 \ . \qquad (52)$$

Here,

$$K_{mn} = \frac{1}{\Lambda_n} \int_0^{\infty} f_m'(z)\, f_n(z)\, dz \ . \qquad (53)$$

Adding Eqs. (51) and (52) yields:

$$A_n' + ikS_n A_n + \frac{S_n'}{2S_n}\left(A_n - B_n\right) + \frac{1}{2}\sum_{m=1}^{\infty}\left[A_m\left(1 + \frac{S_m}{S_n}\right)\right.$$
$$\left. + B_m\left(1 - \frac{S_m}{S_n}\right)\right]\, K_{mn} = 0 \ . \qquad (54)$$

Subtracting those equations from each other gives

$$B_n' - ikS_nB_n - \frac{S_n'}{2S_n}\left(A_n - B_n\right) + \frac{1}{2}\sum_{m=1}^{\infty}\left[A_m\left(1 - \frac{S_m}{S_n}\right)\right.$$

$$\left. + B_m\left(1 + \frac{S_m}{S_n}\right)\right]K_{mn} = 0 \ . \tag{55}$$

Now we define A and B in terms of a and b, which are functions that vary more slowly with respect to x, and we let

$$A_n = \frac{a_n(x)}{\sqrt{S_n(x)}} \ e^{-ik\int_0^x S_n(x')\,dx'} \ , \tag{56}$$

and

$$B_n = \frac{b_n(x)}{\sqrt{S_n(x)}} \ e^{ik\int_0^x S_n(x')\,dx'} \ . \tag{57}$$

Thus Eqs. (54) and (55) become

$$a_n' - \frac{1}{2}\frac{S_n'}{S_n} \ b_n \ e^{2ik\int_0^x S_n(x')\,dx'}$$

$$+ \frac{1}{2}\sum_{m=1}^{\infty}\left\{\left[\frac{S_n + S_m}{\sqrt{S_n S_m}}\right] a_m \ e^{-ik\int_0^x \left[S_m(x')-S_n(x')\right]\,dx'}\right.$$

$$\left. + \left[\frac{S_n - S_m}{\sqrt{S_n S_m}}\right] b_m \ e^{ik\int_0^x \left[S_m(x') + S_n(x')\right]\,dx'}\right\}K_{mn} = 0 \ , \tag{58}$$

45

$$b_n' - \frac{1}{2} \frac{S_n'}{S_n} a_n e^{-2ik \int_0^x S_n(x')\, dx'}$$

$$+ \frac{1}{2} \sum_{m=1}^{\infty} \left\{ \left(\frac{S_n - S_m}{\sqrt{S_n S_m}} \right) a_m e^{-ik \int_0^x \left[S_m(x') + S_n(x') \right] dx'} \right.$$

$$+ \left. \left(\frac{S_n + S_m}{\sqrt{S_n S_m}} \right) b_m e^{ik \int_0^x \left[S_m(x') - S_n(x') \right] dx'} \right\} K_{mn} = 0 \ . \qquad (59)$$

Equations (56) and (57) would be the WKB approximation if $a_n(x)$ and $b_n(x)$ were constants. Thus, Eqs. (58) and (59) become the second-order WKB approximation. Up to this point, we have made no approximations. On pp. 66-68 we show by direct calculation that the reflection term is very small. Therefore, we can neglect reflections. We can now set $b_m = 0$ in Eq. (58).

Removing the <u>n</u>th term from the summation in Eq. (58) yields:

$$a_n' + a_n K_{nn} + \frac{1}{2} \sum_{\substack{m=1 \\ m \neq n}}^{\infty} \left(\frac{S_n + S_m}{\sqrt{S_m S_n}} \right) a_m e^{-ik \int_0^x \left[S_m(x') - S_n(x') \right] dx'} K_{mn} = 0 \ .$$

$$(60)$$

That reduces to a very simple form if we let

$$a_n(x) = \alpha_n(x) e^{- \int_0^x K_{nn}\, dx'} \ . \qquad (61)$$

Recall that, from Eq. (53),

$$K_{nn}(x) = \frac{1}{\Lambda_n} \int_0^\infty f_n'(z) \, f_n(z) \, dz \; . \tag{62}$$

However, from Eq. (47) we see that

$$\Lambda_n'(x) = 2 \int_0^\infty f_n'(z) \, f_n(z) \, dz \; . \tag{63}$$

So,

$$K_{nn} = \frac{1}{2\Lambda_n} \Lambda_n' \; , \tag{64}$$

and hence,

$$\int_0^x K_{nn} \, dx = \frac{1}{2} \ln \left[\Lambda_n(x)/\Lambda_n(0) \right] \; . \tag{65}$$

Thus Eq. (61) is

$$a_n(x) = \alpha_n(x) \sqrt{\frac{\Gamma_n(0)}{\Gamma_n(x)}} \; . \tag{66}$$

So, from Eq. (60) it follows:

$$\alpha_n'(x) = \sum_{\substack{m=1 \\ m \neq n}}^\infty g_{nm}(x) \, \alpha_m(x) \; , \tag{67}$$

where for, $m \neq n$,

47

$$g_{nm}(x) = -\frac{1}{2}\left[\frac{S_n + S_m}{\sqrt{S_m\,S_n}}\right]\sqrt{\frac{\Lambda_m(0)}{\Lambda_m(x)}\frac{\Lambda_n(x)}{\Lambda_n(0)}}$$

$$\times\, e^{-ik\int_0^x \left(S_m - S_n\right)\,dx'}\,K_{mn}\ . \tag{68}$$

We show below that the function K_{mn} (when $m \neq n$) has the form:

$$K_{mn} = \frac{1}{\Lambda_n}\,\frac{1}{ik}\,\frac{1}{c_n^2 - c_m^2}\,\frac{\partial}{\partial x}\,\zeta(x)\ , \tag{69}$$

where $\zeta(x) = q_g(x)$ for the TE case, or $\zeta(x) = Z_g(x)$ for the TM.

Thus putting Eq. (69) into Eq. (68) we get

$$g_{nm}(x) = \frac{1}{2ik}\,\frac{e^{-ik\int_0^x\left(S_m - S_n\right)dx'}}{\sqrt{S_n\,S_m}\left(S_m - S_n\right)}\,\sqrt{\frac{\Lambda_m(0)}{\Lambda_n(0)}\,\frac{\zeta'(x)}{\sqrt{\Lambda_n(x)\,\Lambda_m(x)}}}\ . \tag{70}$$

Here, we used

$$c_n^2 - c_m^2 = 1 - c_m^2 - \left(1 - c_n^2\right) = S_m^2 - S_n^2 = \left(S_m - S_n\right)\left(S_m + S_n\right)\ . \tag{71}$$

We can integrate Eq. (67) directly, then:

$$\alpha_n(x) = \alpha_n(0) + \sum_{\substack{m=1 \\ m\neq n}}^{\infty}\int_0^x g_{nm}(x')\,\alpha_m(x')\,dx'\ . \tag{72}$$

48

We can solve Eq. (72) as we would a perturbation or scattering series. That is, we can use Eq. (72) to find $\alpha_m(x')$ and substitute this into the integral, getting:

$$\alpha_n(x) = \alpha_n(0) + \sum_{\substack{m=1 \\ m \neq n}}^{\infty} \alpha_m(0) \int_0^x g_{nm}(x')\ dx'$$

$$+ \sum_{\substack{m=1 \\ m \neq n}}^{\infty} \sum_{\substack{\ell=1 \\ \ell \neq m}}^{\infty} \int_0^x dx'\ g_{nm}(x') \int_0^{x'} g_{m\ell}(x'')\ \alpha_\ell(x'')\ dx''\ .$$

$$(73)$$

We can repeat this process an arbitrary number of times. If we define $g_{nn}(x) = 0$, and assume summation over repeated symbols, the notation is simpler:

$$\alpha_n(x) = \alpha_n(0) + G_{nm}^{(1)}\ \alpha^m(0) + G_{nm}^{(2)}\ \alpha^m(0) + G_{nm}^{(3)}\ \alpha^m(0) + \cdots \quad (74)$$

where

$$G_{nm}^{(1)}(x) = \int_0^x g_{nm}(x)\ dx\ , \quad (75)$$

$$G_{nm}^{(2)}(x) = \sum_\ell \int_0^x dx'\ g_{n\ell}(x') \int_0^{x'} g_{\ell m}(x'')\ dx'' \quad (76)$$

$$= \sum_\ell \int_0^x dx'\ g_{n\ell}(x')\ G_{\ell m}^{(1)}(x')\ , \quad (77)$$

49

or, in general:

$$G_{nm}^{(i)}(x) = \sum_{\ell} \cdots \sum_{k} \int_0^x dx' \, g_{n\ell}(x') \cdots \int_0^{x''} dx''' \, g_{km}(x''')$$

(78)

$$= \sum_{\ell} \int_0^x dx' \, g_{n\ell}(x') \, G_{\ell m}^{(i-1)}(x') \, .$$

(79)

For $x = 0$, and ignoring reflections, we have, from Eq. (44):

$$F_y = \sum_{n=1}^{\infty} \Gamma_n f_n(z) \, .$$

(80)

At $x = 0$, we have, from Eq. (45):

$$F_y = \sum_{n=1}^{\infty} f_n(z, 0) \, A_n(0) \, .$$

(81)

These must be equal. So, since from Eq. (56) and Eq. (61)

$$A_n(0) = a_n(0)/\sqrt{S_n(0)} = \alpha_n(0)/\sqrt{S_n(0)} \, ,$$

(82)

we see that

$$\alpha_n(0) = \Gamma_n \sqrt{S_n(0)} \, .$$

(83)

That is the initial condition on α.

50

Putting this all together gives, for $0 \leq x \leq \ell$,

$$F_y(x, z) = \sum_{n=1}^{\infty} \Gamma_n \left[1 + Q_n(x)\right] \sqrt{\frac{S_n(0)\, \Lambda_n(0)}{S_n(x)\, \Lambda_n(x)}} \; f_n(x, z) \; e^{-ik \int_0^x S_n(x')\, dx'} \; .$$
(84)

This is Eq. (7) of Sec. 3. In Eq. (84), we define the mode-coupling factor Q_n as:

$$Q_n = \sum_i Q_n^{(i)} \; ,$$
(85)

and

$$Q_n^{(i)}(x) = \sum_{\substack{m=1 \\ m \neq n}}^{\infty} G_{nm}^{(i)}(x) \sqrt{\frac{S_m(0)}{S_n(0)}} \; \frac{\Gamma_m}{\Gamma_n} + G_{nn}^{(i+1)} \; .$$
(86)

Here $Q_n^{(i)}$ represents the $\underline{i}$th order scattering. In the limit, as Γ_n goes to zero, we have:

$$\Gamma_n \left[1 + Q_n(x)\right] = \sum_{m=1}^{\infty} \sum_{i=1}^{\infty} G_{nm}^{(i)}(x) \sqrt{\frac{S_m(0)}{S_n(0)}} \; \Gamma_m \; .$$
(87)

HEIGHT GAIN AND MODAL EQUATIONS.

TE Case.

In the TE case, we write the height-gain function as $e_n(z)$. Recall that it is a solution to Eq. (46). The boundary conditions require that e_n and

$$\dot{e}_n = \frac{1}{ik} \frac{\partial}{\partial z} e_n \qquad (88)$$

be continuous across the boundaries at $z = 0$ and $z = h$. Thus, we can define an impedance function:

$$Z(z) = \frac{e_n(z)}{\dot{e}_n(z)} . \qquad (89)$$

Therefore, the boundary conditions are

$$Z(0) = \frac{1}{q_g} = Z_g , \qquad (90)$$

and

$$Z(h) = -\frac{1}{q_i} = -Z_i . \qquad (91)$$

The solutions of Eq. (46) that satisfy Eq. (90), Eq. (91), and the radiation condition (i.e., that the field must go to zero at infinity), and have $e_n(0) = 1$ are:

$$e_n = \begin{cases} \dfrac{Z_i}{Z_g} \left(\dfrac{CZ_g - 1}{CZ_i + 1} \right) e^{-iCkh} e^{-iq_i k(z-h)} & \text{for } z \geq h , \qquad (92) \\[3ex] \cos Ckz + i \dfrac{q_g}{C} \sin Ckz & \text{for } 0 < z < h , \qquad (93) \\[3ex] e^{iq_g kz} & \text{for } z \leq 0 . \qquad (94) \end{cases}$$

Recall that the solution to Eq. (46) is a superposition of up- and down-going waves whose amplitudes are constants to be determined by the boundary conditions. Thus, in the three regions there are six

constants. Two of them are determined by the radiation condition and one by the normalization condition. In reality, the boundary conditions at $z = 0$ and $z = h$ determine four more constants, but there are only three to be determined. That fact places a restriction on the value of C, which is expressed by the modal equation:

$$\frac{CZ_g + 1}{CZ_g - 1} = \frac{CZ_i - 1}{CZ_i + 1} \, e^{-2iCkh} \quad .$$
(95)

Note that we can write Eq. (95) as

$$iC\left(Z_i + Z_g\right) \cos Ckh = \left(1 + C^2 Z_i Z_g\right) \sin Ckh \quad .$$
(96)

The last form is particularly easy to solve numerically. When σ_g is very large, Z_g is very small, so:

$$iCZ_i \cos Ckh \approx \sin Ckh \quad .$$
(97)

To zeroth order in Z_i, $C_n^{(0)} \approx n\pi/kh$, while to first order

$$C_n^{(1)} \approx C_n^{(0)} \left[\frac{1}{1 - iZ_i/kh}\right] \quad .$$
(98)

We solve Eq. (96) numerically using the Newton-Raphson method starting with $C = C_n^{(1)}$.

TM Case.

In this case, the height-gain function is written as $h_n(z)$ and the boundary conditions require that h_n and

$$\dot{h}_n = -\frac{1}{ikn^2} \frac{\partial}{\partial z} h_n$$
(99)

be continuous across the boundaries. Thus,

$$Z_n(z) = \frac{\dot{h}_n(z)}{h_n(z)} \tag{100}$$

must also be continuous. The boundary conditions are then:

$$Z(0) = -\frac{q_g}{n_g^2} = -Z_g , \tag{101}$$

and

$$Z(h) = \frac{q_i}{n_i^2} = Z_i . \tag{102}$$

This gives:

$$h_n(z, x) = \begin{cases} \dfrac{C - Z_g}{C + Z_i} e^{-iCkh} e^{-iq_i k(z-h)} & \text{for } z \geq h , \tag{103} \\[3ex] \cos Ckz + i \dfrac{Z_g}{C} \sin Ckz & \text{for } 0 < z < h, \tag{104} \\[3ex] e^{iq_g kz} & \text{for } z \leq 0 , \tag{105} \end{cases}$$

and the modal equation

$$\frac{C + Z_g}{C - Z_g} = \frac{C - Z_i}{C + Z_i} e^{-2iCkh} . \tag{106}$$

Equation (106) may also be written:

54

$$iC\left(Z_i + Z_g\right) \cos Ckh = \left(C^2 + Z_iZ_g\right) \sin Ckh \ . \tag{107}$$

The zeroth order solution for small Z_g is then

$$C_n^{(0)} = \left(n - \frac{1}{2}\right) \frac{\pi}{kh} \ , \tag{108}$$

and the first order is

$$C_n^{(1)} = C_n^{(0)} \left(1 - \frac{1}{1 + iZ_ikh}\right) \ . \tag{109}$$

ORTHOGONALITY OF MODES.

To prove the orthogonality of $f_n(z, x)$ we note that, since f_n is a solution of Eq. (46), we can write:

$$f_m \frac{\partial^2}{\partial z^2} f_n - f_n \frac{\partial^2}{\partial z^2} f_m + k^2 \left(C_n^2 - C_m^2\right) f_nf_m = 0 \ . \tag{110}$$

If $n \neq m$, then

$$\int_0^\infty f_nf_m \, dx = \frac{1}{k^2\left(C_n^2 - C_m^2\right)} \int_0^\infty \frac{\partial}{\partial z} \left(f_m \frac{\partial}{\partial z} f_n - f_n \frac{\partial}{\partial z} f_m\right) \, dz \ . \tag{111}$$

The radiation condition ensures that $f_m \to 0$ as $z \to \infty$. The fact that f_m and $\partial f_n/\partial z$ are continuous across the boundary at $z = h$ means that there is no contribution to the integral at $z = h$. If the lower limit of the integral goes to $-\infty$, then clearly, Eq. (111) would reduce to zero. However, using the current limits, since $f_n(0) = 1$, Eq. (111) reduces to:

$$\int_0^\infty f_n(z) f_m(z) \ dz = \frac{-1}{k^2 \left(c_n^2 - c_m^2 \right)} \left[\frac{\partial}{\partial z} f_m(0) - \frac{\partial}{\partial z} f_n(0) \right] \ . \qquad (112)$$

However, from Eq. (93), we see that in the TE case:

$$\frac{\partial}{\partial z} f_m(0) = ikq_g \ , \qquad (113)$$

and, from Eq. (104), in the TM case:

$$\frac{\partial}{\partial z} f_m(0) = ikZ_g \ . \qquad (114)$$

Since we assume both are independent of the mode, this gives us orthogonality.

FUNCTIONS $\Lambda_n(x)$ AND $K_{nm}(x)$.

We calculate $\Lambda_n(x)$ directly from Eq. (47) and from the functional forms of $f_n(z, x)$. In the TE case, we use Eqs. (92) and (93). So after some manipulation and using Eq. (95), the modal equation, we get:

$$\Lambda_n(x) = \frac{1}{2ik} \left\{ - \frac{q_g}{c^2} + \left(ikh + Z_i \right) \left[1 - \left(\frac{q_g}{c} \right)^2 \right] \right\} \ . \qquad (115)$$

In the TM case, using Eqs. (103), (104), and (106) we get:

$$\Lambda_n(x) = \frac{1}{2ik} \left\{ - \frac{Z_g}{c^2} + \left[ikh + \left(\frac{c^2}{q_i n_i^2} - Z_i \right) \frac{1}{c^2 - Z_i^2} \right] \left[1 - \left(\frac{Z_g}{c} \right)^2 \right] \right\} \ . \qquad (116)$$

To compute $K_{nm}(x)$ for $n \neq m$, we start from Eq. (46) and take the derivative with respect to x. The result is:

$$\frac{\partial^2}{\partial z^2} f_n' + 2k^2 q_n' f_n + k^2 q_n^2 f_n' = 0 \ . \tag{117}$$

Multiplying Eq. (46) for mode m by f_n' and subtracting Eq. (117) multiplied by f_m yields:

$$f_m \frac{\partial^2}{\partial z^2} f_n' - f_n' \frac{\partial^2}{\partial z^2} f_m + 2k^2 q_n' q_n f_n f_m + k^2 \left(q_n^2 - \sigma^2 \right) f_n' f_m = 0 \ . \tag{118}$$

Assuming $n \neq m$:

$$\int_0^\infty f_n' f_m \, dz = - \frac{1}{k^2 \left(c_n^2 - c_m^2 \right)} \int_0^\infty dz \, \frac{\partial}{\partial z} \left(f_m \frac{\partial}{\partial z} f_n' - f_n' \frac{\partial}{\partial z} f_m \right) \ , \tag{119}$$

which gives (after due attention to the boundary conditions):

$$K_{nm} = - \frac{1}{\Lambda_m} \frac{1}{k^2 \left(c_m^2 - c_n^2 \right)} \left(\frac{\partial f_n'}{\partial z} - f_n' \frac{\partial f_m}{\partial z} \right) \Bigg|_{z=0} \ . \tag{120}$$

If we write

$$f_n(z, x) = \cos Ckz + \frac{\zeta(\bar{x})}{C} \sin Ckz \ , \tag{121}$$

then Eq. (120) becomes

$$K_{nm} = + \frac{1}{\Lambda_m} \frac{1}{ik \left(c_m^2 - c_n^2 \right)} \frac{\partial}{\partial x} \zeta(x) \ , \tag{122}$$

where $\zeta(x) = q_g$ in the TE case and $\zeta(x) = Z_g$ in the TM.

57

MODE COUPLING AT SHARP BOUNDARY.

Using an adaptation of the method of Pappert and Shockey [1972],
we can compare our method with the results from methods using a sharp
boundary.

First we write F_{yn} and F_{zn} as the y and z components of the field
of the nth mode. In the TE case, we take $F_z = H_z$ and in the TM case,
$F_z = -E_z$. If we write:

$$
\hat{L} = \begin{pmatrix} 0 & 1 \\ 1 + \dfrac{1}{k^2}\dfrac{\partial^2}{\partial z^2} & 0 \end{pmatrix} \quad , \tag{123}
$$

and

$$
\vec{u}_n = \begin{pmatrix} F_{yn} \\ F_{zn} \end{pmatrix} \quad , \tag{124}
$$

then Maxwell's equations can be written:

$$
\hat{L}\vec{u}_n = -\frac{1}{ik}\frac{\partial}{\partial x}\vec{u}_n \quad . \tag{125}
$$

If n_g^2 is not a function of x, then x appears only in an exponential
term, as for example;

$$
u_{yn} = \Gamma_n f_n(z)\, e^{-ikS_n x} \quad . \tag{126}
$$

So Eq. (125) becomes:

$$
\hat{L}\vec{u}_n = S_n \vec{u}_n \quad . \tag{127}
$$

Now we define $\vec{v}_n$ to be eigenvectors of $\hat{L}^\dagger$, the transpose of $\hat{L}$, and we

introduce the following bracket notation, for arbitrary vector functions $\vec{r}(z)$ and $\vec{s}(z)$

$$\langle \vec{r}, \vec{s} \rangle = \int_0^\infty \vec{r}(z) \cdot \vec{s}(z) \ dz \ . \tag{128}$$

Now it is clear that

$$\langle \vec{v}_m, \hat{L}\vec{u}_n \rangle = \langle \hat{L}^\dagger \vec{v}_m, \vec{u}_n \rangle \tag{129}$$

If we let the eigenvalue of $\vec{v}_m$ be ν_m so

$$\hat{L}^\dagger \vec{v}_m = \nu_m \vec{v}_m \ , \tag{130}$$

then Eq. (129) becomes:

$$S_n \langle \vec{v}_m, \vec{u}_n \rangle = \nu_m \langle \vec{v}_m, \vec{u}_n \rangle \ . \tag{131}$$

Finally we see:

$$S_n = \nu_n \quad \text{and} \quad \langle \vec{v}_m, \vec{u}_n \rangle = 0 \quad \text{if } n \neq m \ . \tag{132}$$

It is clear that

$$\vec{v}_m = \begin{pmatrix} F_{zm} \\ F_{ym} \end{pmatrix} \ , \tag{133}$$

so,

$$\langle \vec{v}_m, \vec{u}_n \rangle = \int_0^\infty \left(F_{zm}, \ F_{ym} \right) \cdot \begin{pmatrix} F_{yn} \\ F_{zn} \end{pmatrix} dz = \int_0^\infty \left(F_{ym} F_{zn} + F_{zm} F_{yn} \right) dz \ .$$

$$(134)$$

Therefore, since $F_{zm} = S_n F_{yn}$ [Eq. (127)],

$$\langle \vec{v}_m, \ \vec{u}_n \rangle = \left(S_n + S_m \right) \int_0^\infty F_{ym} F_{yn} \ dz \tag{135}$$

$$= 2 \ S_m \tilde{\Lambda}_m \delta_{mn} \ . \tag{136}$$

For the case of waves on both sides of the boundary, let $\vec{u}_n^-$ represent the wave before the boundary and $\vec{u}_n^+$ represent the wave after it. Now the boundary condition (that F_y and F_z be continuous) is expressed as

$$\sum_{n=1}^\infty \vec{u}_n^- = \sum_{n=1}^\infty \vec{u}_n^+ \ . \tag{137}$$

If we multiply by $\vec{v}_m^+$ and integrate from 0 to ∞, we find that:

$$\sum_{n=1}^\infty \langle \vec{v}_m^+, \ \vec{u}_n^- \rangle = \sum_{n=1}^\infty \langle \vec{v}_m^+, \ \vec{u}_n^+ \rangle \ . \tag{138}$$

From Eq. (134) it is clear that:

$$\langle \vec{u}_m^+, \ \vec{v}_n^- \rangle = \left(S_m^+ + S_n^- \right) \int_0^\infty F_{ym}^+ F_{yn}^- \ dz \tag{139}$$

$$= \left(S_m^+ + S_n^- \right) \tilde{X}_{mn} \ . \tag{140}$$

60

Using Eq. (136), the result is:

$$2S_m^+ \, \widetilde{\Lambda}_m^+ = \sum_{n=1}^{\infty} \left(S_m^+ + S_n^- \right) \widetilde{X}_{mn}. \tag{141}$$

Now, using Eq. (126) we get:

$$\widetilde{\Lambda}_m^+ = \int_0^{\infty} \left(\Gamma_m^+ \right)^2 \, f_n^+(z) f_m^+(z) \, e^{-2ikS_n x} \, dz \tag{142}$$

$$= \left(\Gamma_m^+ \right)^2 \, e^{-2ikS_m^+ x} \, \Lambda_m^+ \, , \tag{143}$$

where Λ_m^+ was previously defined [see Eq. (47)]. Now we write:

$$\widetilde{X}_{mn} = \int_0^{\infty} \Gamma_m^+ \, \Gamma_n^- \, f_m^+(z) f_n^-(z) \, e^{-ik\left(S_m^+ + S_n^- \right) x} \, dz \tag{144}$$

$$= \Gamma_m^+ \, \Gamma_n^- \, X_{mn} \, e^{-ik\left(S_m^+ + S_n^- \right) x} \, , \tag{145}$$

and it follows that:

$$\Gamma_m^+ = \frac{1}{2\Lambda_m^+} \sum_{n=1}^{\infty} \left[1 + \frac{S_n^-}{S_m^+} \right] \Gamma_n^- \, X_{mn} \, e^{ik\left(S_m^+ - S_n^- \right) x} \, . \tag{146}$$

Consider:

$$X_{mn} = \int_0^{\infty} f_m^+ f_n^- \, dz \, . \tag{147}$$

61

From Eq. (46) we now have:

$$f_m^+ \frac{\partial^2}{\partial z^2} f_n^- - f_n^- \frac{\partial^2}{\partial z^2} f_m^+ + k^2 \left[\left(c_n^- \right)^2 - \left(c_m^+ \right)^2 \right] f_m^+ f_n^- = 0 \ . \tag{148}$$

However, we have solved equations in this form before, so it follows:

$$\int_0^\infty f_m^+ f_n^- \, dz = \frac{-1}{ik \left[\left(c_n^- \right)^2 - \left(c_m^+ \right)^2 \right]} \left(\zeta^- - \zeta^+ \right) \ . \tag{149}$$

Thus the connecting formula across a sharp boundary at x is:

$$\Gamma_m^+ = \frac{1}{2ik} \frac{1}{S_m^+ \Lambda_m^+} \sum_{n=1}^{\alpha} \Gamma_n^- \left[\frac{\zeta_m^+ - \zeta_n^-}{S_m^+ - S_n^-} \right] e^{ik\left(S_m^+ - S_m^- \right)x} \ . \tag{150}$$

RESULTS FOR TE.

Results for the TM case are presented in Sec. 4, in this subsection, we discuss some results for the TE case. In the TE case, we are allowed to make some approximations that give us analytic solutions for some important quantities. Unfortunately, we cannot find such solutions in the TM case and so must proceed numerically. First, we consider the derivative of Z_i and C with respect to x, recalling that

$$q_i^2 = n_i^2 - 1 + c^2 \ . \tag{151}$$

It follows that

$$q_i q_i' = CC' \ . \tag{152}$$

Thus,

$$Z_i' = -\frac{1}{q_i^2} q_i' = -Z_i^3 \, CC' \quad . \tag{153}$$

To find C', we take the derivative of the modal equation [Eq. (95)] and find that

$$CC'\left\{\left[ikh + Z_i\right]\left[1 - \left(\frac{q_g}{C}\right)^2\right] - \frac{q_g}{C}\right\} = Z_g'/Z_g^2 \quad . \tag{154}$$

Comparing this to Eq. (115) shows:

$$C' = \frac{1}{2ik \, \Lambda_n} \, \frac{1}{CZ_g^2} \, Z_g' \quad . \tag{155}$$

In Eq. (154), the $(q_g/C)^2$ dominates, and since $|Z_i| \ll |kh|$, then

$$-\frac{1}{C} \, C' \, ikh \approx Z_g' \quad . \tag{156}$$

We integrate this directly to get

$$C(x) = C_0 \, e^{+\frac{i}{kh}\left[Z_g(x) - Z_g(0)\right]} \quad . \tag{157}$$

Equation (157) has been compared to the numerical solution of the modal equation [Eq. (95)] at 5, 25, and 50 kHz, and is valid to less than 0.1 percent over a range in σ_g from 4 S/m down to 10^{-5} S/m.

We can use the above to study the coupling of TE modes. From Eq. (60) it is clear than K_{mn}/K_{nn} (where $m \neq n$) is the relative amount of mode m coupled into mode n by the conductivity change from x to x + dx. In this section we show that this is always very small, and hence, that TE mode coupling is very small, as expected.

If we use the same reasoning as above, Eq. (115) can be approximated as

$$\Lambda_n \approx \frac{1}{2} h \left[\frac{q_g}{C}\right]^2 , \qquad (158)$$

then Eq. (122) becomes, for the TE case (recall $m \neq n$)

$$K_{nm} \approx \frac{2}{kh} \left(C_m Z_g\right)^2 \frac{1}{\left(C_m^2 - C_n^2\right)} q_g' \quad . \qquad (159)$$

The diagonal term is

$$K_{nn} = \frac{1}{2\Lambda_n} \Lambda_n' . \qquad (160)$$

So we have

$$K_{nn} \approx \left[\frac{q_g'}{q_g} - \frac{C_n'}{C_n}\right] \quad . \qquad (161)$$

Thus, using Eq. (156) we get

$$K_{nn} \approx \frac{q_g'}{q_g} \left(1 + \frac{1}{ikhq_g}\right) \approx \frac{q_g'}{q_g} . \qquad (162)$$

This approximation appears to be very accurate (greater than three decimal places at 20 kHz), when compared to the complete equation.

Dividing Eq. (159) by Eq. (162) yields:

$$\left| \frac{K_{nm}}{K_{nn}} \right| \approx \left| \frac{2i}{kh} Z_g \frac{C_m^2}{C_m^2 - C_n^2} \right| \ll 1 . \qquad (163)$$

Thus, the off-diagonal terms are very small and we do not expect a large amount of mode coupling for the TE modes. In fact, using Eq. (157) it is fairly easy to show that Eq. (70) reduces to

$$g_{nm}(x) = \frac{2}{ikh} \frac{n^2}{m^2 - n^2} \frac{1}{\sqrt{S_m(0) \, S_n(0)}} \frac{q_g'}{q_g^2} \; . \tag{164}$$

Therefore,

$$G_{nm}^{(1)} = \frac{2}{ikh} \frac{n^2}{m^2 - n^2} \frac{1}{\sqrt{S_m(0) \, S_n(0)}} \left[Z_g(x) - Z_g(0) \right] \, , \tag{165}$$

and

$$G_{nm}^{(2)} \propto \frac{Z_g^2(x) - Z_g^2(0)}{(kh)^2} \; . \tag{166}$$

Using Eq. (86), we find that $1 + Q_n(x) \approx 1$. The total field, then, is

$$E_y(z, \, x) \approx \sum_{n=1}^{\infty} \Gamma_n \sqrt{\frac{S_n(0)}{S_n(x)}} \sqrt{\frac{\Lambda_n(0)}{\Lambda_n(x)}} \; e_n(z, \, x) \; e^{-ik \int_0^x S_n(x') \, dx'} \; . \tag{167}$$

We know, however, that

$$\sqrt{\frac{\Lambda_n(0)}{\Lambda_n(x)}} \approx \frac{q_g(0)}{C_n(0)} \frac{C_n(x)}{q_g(x)} \, , \tag{168}$$

and

65

$$e_n(z, \ell) \approx \frac{q_g(\ell)}{C_n(\ell)} \sin Ckh \ , \qquad (169)$$

so it follows that

$$\sqrt{\frac{\Lambda_n(0)}{\Lambda_n(\ell)}} \ e_n(z, \ell) \approx \frac{q_g(0)}{C_n(0)} \frac{C_n(\ell)}{q_g(\ell)} \frac{q_g(\ell)}{C_n(\ell)} \ \sin Ckh \qquad (170)$$

$$\approx e_n(z, 0) \ .$$

We see, therefore, that the field has not changed significantly across the boundary.

REFLECTIONS.

In this subsection, we consider the reflection term b_n in Eq. (58) and (59). We do this by defining a reflection coefficient R such that

$$b_n = R_n \alpha_n \ e^{- \int_0^x K_{nm} \ dx'} \ . \qquad (171)$$

With this definition, Eqs. (58) and (59) can be combined into

$$R_n' = - \frac{S_n'}{2S_n} \left[R^2 \ e^{2ik \int_0^x S \ dx'} \ - e^{-2ik \int_0^x S \ dx'} \right]$$

$$- \frac{1}{2} \sum_{\substack{m=1 \\ m \neq n}}^{\infty} \left[\left(R_n - R_m \right) g_{nm} + \left(i - R_m R_n \right) \tilde{g}_{nm} \right] \frac{\alpha_m}{\alpha_n} = 0 \ ,$$

$$(172)$$

where

$$\tilde{g}_{nm} = \frac{S_n - S_m}{S_n + S_m} g_{nm} \quad . \tag{173}$$

The terms in the summation account for mode coupling and are clearly second order. We have shown that, at least for TE, they can be ignored. Thus, if we ignore mode coupling, we get:

$$R(x) = \int_x^\ell \frac{S'}{2S} e^{-2ik \int_0^{x'} S \, dx''} dx' \quad . \tag{174}$$

[This form gives $R(\ell) = 0$, as required, since there can be no reflected wave past $x = \ell$.] To determine the magnitude of R, notice that the exponential term in Eq. (174) is less than one due to the imaginary part of S (the attenuation). Since we do not expect the attenuation to significantly affect the wave in the short distance of the boundary, we write:

$$R(x) \leq \int_x^\ell \frac{S'}{2S} \, dx' \quad , \tag{175}$$

which we solve directly as:

$$R(x) \leq \frac{1}{2} \ln [S(\ell)/S(x)] \quad . \tag{176}$$

The maximum reflections occur at $x = 0$, so,

$$R(x) \leq R(0) \leq \frac{1}{2} \ln [S(\ell)/S(0)] \quad . \tag{177}$$

Using the approximation for the TE mode--Eq. (157)--we can show (after some manipulation), that if the change in Z_g across the boundary is ΔZ_g, then

$$R \approx \frac{i}{2kh} \Delta Z_g \left(\frac{C_0}{S_0}\right)^2 \ . \tag{178}$$

Thus, the condition for negation of reflection is:

$$\frac{1}{2} \frac{1}{kh} \left| \Delta Z_g \right| \left| \frac{C_0}{S_0} \right|^2 \ll 1 \ . \tag{179}$$

That condition is met in the TE case by all reasonable boundaries.

For the TM case, we can calculate the first-order term directly. The reflection term $|R|$ is the largest for the Brewster's mode where $C \approx Z_g$. For a frequency of 30 kHz, $|R| \approx 0.02$ and changes little over the VLF range.

DISTRIBUTION LIST

DEPARTMENT OF DEFENSE

DEFENSE COMMUNICATIONS AGENCY
    ATTN. P CROWLEY
3 CYS ATTN: A BLANKFIELD

DEFENSE INTELLIGENCE AGENCY
2 CYS ATTN: RTS-2B

DEFENSE NUCLEAR AGENCY
3 CYS ATTN: RAAE
4 CYS ATTN: TITL

DEFENSE NUCLEAR AGENCY
    A.'TN: TDNM-CF
    ATTN: TDTT W SUMMA

DEFENSE TECHNICAL INFORMATION CENTER
12 CYS ATTN: DD

DEPARTMENT OF THE NAVY

NAVAL OCEAN SYSTEMS CENTER
    ATTN: CODE 544

NAVAL RESEARCH LABORATORY
    ATTN: CODE 4183 F KELLY

NAVAL UNDERWATER SYSTEMS CENTER
    ATTN: CODE 3411 J KATAN

DEPARTMENT OF THE AIR FORCE

AIR FORCE ELECTRONIC WARFARE CENTER
    ATTN: LT M MCNEELY

AIR FORCE GEOPHYSICS LABORATORY
    ATTN: LID/J RAMUSSEN

AIR FORCE WEAPONS LABORATORY
    ATTN: NTAAB
    ATTN: SUL

AIR UNIVERSITY LIBRARY
    ATTN: AUL-LSE

ROME AIR DEVELOPMENT CENTER, AFSC
    ATTN: J TURTLE

STRATEGIC AIR COMMAND
2 CYS ATTN: XRFC

DEPARTMENT OF ENERGY

SANDIA NATIONAL LABORATORIES
    ATTN: TECH LIB

DEPARTMENT OF DEFENSE CONTRACTORS

JOHNS HOPKINS UNIVERSITY
    ATTN: J D PHILLIPS
    ATTN: R LUNNEN

KAMAN SCIENCES CORPORATION
    ATTN: DASIAC

KAMAN TEMPO
    ATTN: B GAMBILL
    ATTN: DASIAC
    ATTN: R RUTHERFORD

LOCKHEED MISSILES & SPACE CO, INC
    ATTN: J HENLEY

MISSION RESEARCH CORP
    ATTN: TECH LIBRARY

PACIFIC-SIERRA RESEARCH CORP
2 CYS ATTN: C WARBER
2 CYS ATTN: E FIELD JR

R & D ASSOCIATES
    ATTN: C GREIFINGER
    ATTN: M GROVER

RAND CORP
    ATTN: C CRAIN

TELECOMMUNICATION SCIENCE ASSOCIATES
    ATTN: R BUCKNER